Orberger, B., Wagner, C., Wirth, R., Quirico, E., Gallien, J. P., Derré, C., Montagnac, G., Noret, A., Jayananda, M., Massault, M., Rouchon, V. (2012): Origin of iron oxide spherules in the banded iron formation of the Bababudan Group, Dharwar Craton, Southern India. - Journal of Asian Earth Sciences, 52, 31-42

DOI: 10.1016/j.jseaes.2012.02.008

Origin of iron oxide spherules in the banded iron formation of the Bababudan Group, Dharwar Craton, Southern India

Beate Orberger[1,**], Christiane Wagner[2], Richard Wirth[3], Eric Quirico[4], Jean Paul Gallien[5], Colette Derré[2], Gilles Montagnac[6], Aurélie Noret[1], Mudlappa Jayananda[7], Marc Massault[1] and Virgile Rouchon[1, †]

[1]Université Paris Sud XI, CNRS-UMR IDES 8148, Département des Sciences de la Terre, Bât. 509, 91405 Orsay Cedex, ERAMET RESEARCH, 1 Avenue Albert Einstein, 78190 Trappes ; France. E-mail : beate.orberger@erametgroup.com

[2]Laboratoire MMM, ISTEP, CNRS-UMR 7193, Université Pierre et Marie Curie-UPMC, 4 Place Jussieu, 75251 Paris Cedex, France

[3]GeoForschungsZentrum Potsdam (GFZ), Department 4, Telegrafenberg, 14482 Potsdam, Germany.

[4]Laboratoire de Planétologie de Grenoble, CNRS-UMR 5109, Université Joseph Fourier, OSUG, Bât. D de Physique, 38041 Grenoble Cedex 9, France

[5]Laboratoire Pierre Süe, CNRS-UMR 9956, CEA-Saclay, 91191 Gif-sur-Yvette, France

[6]Laboratoire de Sciences de la Terre, CNRS-UMR 5570, ENS-Lyon, 46 Av. d'Italie, 69364 Lyon Cedex 07, France

[7] Department of Geology, Centre of Advanced Studies, University of Delhi, Delhi - 110 007, India

† Present address: IFP, Rueil-Malmaison, France

**To whom the correspondence should be addressed and present address

ABSTRACT

The banded iron formation of the Bababudan Group (Western Dhawar Craton, India) is composed of millimetric to centimetric alternating quartz and grey to red Fe-oxide bands. Major phases are quartz and martite (hematized magnetite) with minor Fe-sulfides and Ca-Mg-Fe-carbonates. Micrometric Fe-oxide spherules fill cavities in discontinuous micrometric layers of Fe-oxides that occur in the massive quartz layers and at the interface of massive Fe-oxide and quartz layers. The spherules are composed of micrometric radial plates of hematite intergrown with nanometric magnetite. These spherules contain carbonaceous matter (CM) with nanometric Fe-particles and have low N contents (~ 900 ppm; CM1). The spherule formation is attributed to a low temperature hydrothermal process (150-200°C) at around 2.52 Ga, possibly favored by the presence of CM. These hydrothermal fluids dissolved diagenetic interstitial sulfides or carbonates creating cavities which, provided space for the spherule precipitation. Carbonaceous matter of semi-anthracite maturity is encapsulated in quartz grains adjacent to the Fe-oxide spherules (CM2) and it is thus concluded that CM1 and CM2 are most likely contemporaneous and of the same origin, either incorporated at the time of BIF formation or during the hydrothermal event at 2.52 Ga from the underlying phyllitised black shales. Carbonaceous matter (CM3) was also found around the Fe-oxide spherules and the martite grains. CM3 has much higher N contents (> 5000 ppm) and is of a lower maturity than CM1 and CM2 and is related to weathering, also indicated by the presence of goethite and kaolinite. The $\delta^{13}C$ of all CMs varies from -19.4 to -24.7 ‰, similar to values measured in the underlying phyllitised black shales and likely reflect denitrifying microbial activity.

Keywords: hematite, spherules, banded iron formations, carbonaceous matter, Raman spectroscopy, FIB-TEM,

INTRODUCTION

Iron oxide spherules (α-Fe_2O_3), coexisting with jarosite, were detected on the Martian surface at Meridiani Planum (Christensen, 2000; Christensen, 2001; Klingelhöfer, 2004; Morris, 2006) and were interpreted as being of abiotic origin, as a result of the breakdown of jarosite through groundwater reaction during oxidizing diagenesis (Chan, 2004; McLennan, 2005), or due to

oxidation of primary pyrite by hydrothermal, sulphur-rich solutions (Golden, 2008; Zolotov and Shock, 2005). However, in terrestrial Fe-oxide grains and spherules, organic matter can be present (McConchie, 1987; Klein and Beukes, 1992; Yoshioka et al., 2001; Orberger et al., 2006; Pinti et al., 2007) and thus the Fe-oxide spherules on Mars may represent an important target in the search of biomarkers. Among terrestrial environments, banded iron formations (BIFs) are potential time equivalent analogues. Currently, only two BIF localities are known to host Fe-oxide spherules: 1) spherulitic hematite composed of numerous curved platelets around a central void in the 2.5 Ga old Marra Mamaba formation in the Hamersley Basin, Western Australia, where a colloidal origin due to volume reduction was proposed for the individual spherule formation (Ahn and Buseck, 1990) and 2) the here studied carbonaceous matter bearing Fe-oxide spherules from BIF hosted in the 2.9 Ga Bababudan Group in the Western Dhawar Craton, Southern India. Fe-Mn nodules hosting carbonaceous matter are also known from Archean BIF in Western Australia (Yoshioka et al., 2001).

Fe-oxide spherules can form both abiotically (Fortin, 1998; Ferris et al., 1999) and biotically in hydrothermal (Brasier et al., 2006), shallow coastal and lake settings (Beitler-Bowen et al. 2008; Douglas et al., 2008; Tyler and Buckney, 1980; Tipping et al, 1981; Kappler and Newman, 2004; Halbach, 1986; Zhang et al., 2006). Abiotic, round-shaped Fe-oxides can represent ooids with concentric or radial internal textures (Cornell and Schwertmann, 2003). Experimentally, hematite spherules with a radial fibrous texture, were synthetized from hydrothermal solutions at 150 °C - 200 °C (Golden et al., 2008).

The presence of organic compounds favors the formation of Fe-and Mn-oxides and spherule formation. Based on the presence of biophilic elements (P, N, S), microbial activity was suggested as the mode of formation for Mn-oxide spherules in Death Valley, California, (Douglas et al., 2008). In experimental studies, hematite spherules formed in an organic solution between 200°C-300°C (Zhang et al., 2006) and the preservation of carbonaceous

matter, even in an oxidizing environment, appears to result from its sorption onto magnetite-hematite surfaces, (Mayer et al., 2004; Zimmerman et al., 2004; Salmon et al., 2000).

For the first time, Fe-oxide spherules that include and are surrounded by carbonaceous matter were detected in the Mesoarchean, 500 m thick BIF of the Bababudan group. In this paper we characterize the Fe-oxide spherules and the carbonaceous matter by a combination of micro analytical techniques (scanning electron microscopy, micro Raman spectroscopy, focused ion beam transmission electron microscopy and nuclear reaction analysis), and $\delta^{13}C$ isotopic measurements of individual Fe-oxide and quartz layers. The origin and the timing of formation of the Fe-oxide spherules are discussed.

GEOLOGICAL SETTING

The Dharwar craton (DC) of southern India corresponds to large tilted section of Archean continental crust that show progressive transition from granite-greenstone terrains in the north to granulite terrains to the south (Chadwick et al., 2000; Chardon et al., 2008;Jayananda et al., 2006; Swaminath and Ramakrishnan, 1981; Taylor et al., 1984; Raith et al., 1982; Fig. 1). The craton has been divided into an Eastern (EDC) and a Western Dharwar craton (EDC), based on the nature and abundance of greenstones, crustal thickness, grade of regional metamorphism and degree of melting (Swami Nath et al., 1976; Jayananda et al., 2006; Chardon et al., 2008;Fig. 1A). The steep mylonitic zone along the eastern boundary of the Chitradurga greenstone belt is considered dividing line between two crustal blocks (Jayananda et al., 2006;Chardon et al., 2008). In the WDC, greenstone belts of the Dharwar supergroup (3.0 - 2.6 Ga) are subdivided into the Bababudan Group and the overlying Chitradurga Group (Nutman et al., 1996; Anil Kumar et al., 1996; Swaminath and Ramakrishnan, 1981). Both Bababudan and Chitradurga Group volcano-sedimentary greenstone sequences are affected by varying degree of metamorphism, from greenschist to amphibolite facies (Fig. 1A), which in turn spatially

associated with crustal reworking and emplacement of high-potassic Chitradurga and Arsikere-Banavara plutons at 2.62 ± 0.02 Ga (Jayananda et al., 2006). Laterally to the east 2.62 Ga granulite facies metamorphic event related to the emplacement of the Chitradurga granite have been documented (Jayananda et al., 2011). The major N-S trending shear zones associated with cooling of crust, controlled lower temperature mesothermal (300 °C - 350 °C) gold mineralization during compressional tectonics (Kolb et al., 2004). Recent dating of monazite and xenotime in gold-mineralized quartz veins of the WDC, reveals the age of the last hydrothermal overprint at 2522±6 Ma and 2520± 9 Ma; Sarma et al., 2011).

The studied BIF (# BIF 14A; N 13°19'539'', E 76°42'300''; altitude: 871 m, Fig. 1A; about 2km east of Kibbanahalli cross on the way to temple in the hill top) is located in the Kibbanahalli arm in WDC and belongs to the 2.9 - 2.7 Ga Bababudan Group (Swaminath and Ramakrishnan, 1981;Anil Kumar et al., 1996; Trendall et al., 1997) in the Kibbanahalli arm of Chitradurga Greenstone Belt (Seshadri et al., 1981; Chardon et al., 1996). At the sample location, the lithological succession is typical of the shallow water platform lithologies of the Bababudan Group (Swaminath and Ramakrishnan, 1981; Kumar and Das Sharma, 1998; Srinivasan and Ojakangas, 1986), Fig. 1B). Oligomict conglomerates are overlain by mafic volcanics, phyllites which are followed by thick BIF characterized by alternating millimetric grey Fe-oxide and white quartz layers (Fig. 2A). Although the rocks experienced lower greenschist facies conditions, the primary features of the volcanic rocks and sediments are well preserved. Based on field observations, BIF is interpreted as being a result of hydrothermalism and/or volcaniclastic sedimentation along with biological activity (Gnaneshwar Rao and Naqvi, 1995).

ANALYTICAL METHODS

Microscopy

Five polished thin sections were studied by reflected and transmitted light optical microscopy, and by scanning electron microscopy (using SEM Philips XL 30) connected to an EDX-PGT Ge-detector for semi-quantitative chemical analyses (20 - 30 kV) at the Université de Paris Sud XI, and SEM Zeiss SUPRA 55VP at the Université Pierre et Marie Curie, UPMC, Paris. Focused ion beam (FIB: FEI FIB 2000) transmission electron microscopy (TEM), high-resolution transmission electron microscopy (HRTEM) and electron energy loss-spectroscopy (EELS) on selected sections of Fe-oxide grains were performed at the GeoForschungsZentrum (GFZ, Potsdam, Germany). Polished thin sections and block samples were coated with gold. FIB foils of about 100 nm were cut through the spherules. The crystallography and chemical composition of the Fe-oxides and the carbonaceous matter (CM) within the Fe-oxide spherules was determined by energy-dispersive X-ray analyses (EDX) and electron energy loss spectroscopy (EELS) connected to the TEM. The physical process of the FIB technique and the analytical conditions during TEM analyses are described in Wirth (2004) and references therein.

Nuclear reaction analysis

Nitrogen and carbon were located and quantified on polished sample blocks by Nuclear Reaction Analysis (NRA) at the CEA-CNRS Pierre Süe Laboratory nuclear microprobe (Khodja et al., 2001). A 1.9 MeV deuteron ($^2H^+$) incident beam focused to 3 x 3 μm^2 at 0.8 nA is necessary for nitrogen determination to reach 20 pC-accumulated charge in seven hours. The $^{14}N(d, p_0)^{15}N$ and $^{12}C(d, p_0)^{13}C$ nuclear reactions are used to quantify N and C, respectively. Sample blocks were polished with Al_2O_3 powder, cleaned in an ultrasonic bath and coated with gold. Only signals from 1 to ~ 9 μm depth were used for N and C quantification to avoid surface contamination. The Fe-oxides and quartz were analyzed in scanning mode to select the largest and thickest parts for N and C quantification. The detection limit of N and C by NRA is about 100 ppm. The method, standards used for measurements and the data evaluation from the NRA

and X-ray spectra are described in (Khodja et al., 2001; Daudin and Gallien, 2003; Orberger et al., 2007a; Orberger et al., 2007b; Pinti et al., 2007).

Carbon isotope analyses

Eleven alternating Fe-oxide and quartz layers from the same sample block were separated and cleaned. For one layer (18), fractions enriched in quartz or iron oxide minerals were separated using polytungstate solutions with densities of about 2.7 g cm^{-3}. These separations were performed at the Department of Earth and Planetary Science Laboratory, Osaka University, Japan (Hashizume et al., 2008). Additionally, samples were submitted to carbonate removal by a hydrochloric acid (~ 4% w/v) solution heated to 80°C for 30 minutes, rinsed to a neutral pH with demineralized water and dried overnight at 100 °C. One bulk sample was also analyzed. Two to three hundred mg of each sample powder was introduced into a quartz tube containing a thin (0.65 x 3 mm) copper oxide wire, isolated and evacuated up to 6 x 10^{-3} torr. The sample was then combusted at 850 °C for 30 minutes and the produced gas phase analyzed for the $^{13}C/^{12}C$ ratio using a stable isotope mass spectrometer SIRA 10 of VG Instruments® at the UMR IDES, Université Paris Sud XI. The C-isotope ratios are reported as the ‰ deviation relative to the Vienna Pee Dee Belemnite (V-PDB) international standard (Table 1). Total uncertainties on the measurement are of ± 0.2 ‰.

Micro Raman spectroscopy

Micro Raman spectroscopy was performed at the Laboratoire de Sciences de la Terre, ENS-Lyon, Lyon, France, using two Horiba Jobin-Yvon Labram HR800 spectrometers equipped with microscopes for the backscattered Raman signal collection.

Visible Raman spectroscopy of the oxides. Oxide phases were characterized by visible micro Raman spectroscopy through unpolarized Raman spectra within 30 - 60 s. The excitation

source was an argon ion laser beam at λ = 514.5 nm (2.41 eV). The lateral resolution of the focused laser probe was measured at 1 μm using x100 objective magnitude. The laser power on the sample was less than 5mW. Calibration was performed during measurements in a silicon semiconductor mode at 520.7 cm^{-1}. The spectral resolution was about 4 cm^{-1} (with 600 gr/mm dispersive grating).

UV Raman spectroscopy of the carbonaceous matter. Carbonaceous matter (CM) was studied by ultra violet (UV) micro Raman spectroscopy instead of visible micro Raman spectroscopy to avoid the strong fluorescence background from the sample. The Raman spectra were collected using a 244 nm (5.08 eV) wavelength excitation achieved using a frequency-doubled argon ion laser. Spectra were acquired with an UV-enhanced CCD detector and 50x long working distance or 40x UV objectives providing a spot of 4 - 5 μm across.

Damage to the sample (heating and photostability) are a critical issue in micro Raman spectroscopy, particularly for UV excitation, which requires careful sample preparation and analytical procedure. The Raman spectra were acquired from a polished, uncoated slab of the BIF. To avoid polishing effects to the CM structure, we focused the laser beam on CM beneath the surface of the quartz matrix, as recommended by Pasteris (1989), and deep inside the cavities. Prior to Raman measurements, the presence of CM in cavities was revealed by Raman mapping (see deposit item, supplementary figure 1) and back-scattered electron imaging. A series of coal standards provided by the Penn State Coal Data Bank (Quirico et al., 2005; 2009) and a series of type II kerogen standards (provided by Institut Français du Pétrole – Rueil Malmaison, France) were studied for comparison. Coal and kerogen grains were picked up and crushed between two glass sides (see details of the preparation in Quirico et al., 2005).

In order to determine the acquisition conditions that ensured the lack of visible damage and spectral variations, we collected Raman spectra by varying acquisition times and laser power at the same spot location. The best analytical conditions were: laser power on the sample of about

500 μW to less than 1mW, acquisition time of 240 s to 600 s depending on the CM location, and 3600 gr/mm grating. The absence of a visible burial print was checked after each irradiation. A minimum of 10 spectra was acquired for each sample in the spectral region 800-2000 cm^{-1}. These conditions were applied to all Raman spectra collected from the Indian sample as well as the coal (Quirico et al., 2009) and kerogen standards. Continuous calibration was performed with a diamond at 1331 cm^{-1} during analyses.

The Raman spectra were processed by the PeakFit 4.0 (Jandel Scientific) software. A linear base line correction was applied, and the fitting of the spectral profiles of the D and G bands was performed with a 2-band fit model with a combination of Gaussian and Lorentzian profiles using Voigt functions. Any possible substructures within the D and G bands were ignored in the spectral fitting analysis, which focused on reproducing the overall line shape. The total set of data is available from the authors and Table 2 shows the average results of the fits for CM2 and CM3.

RESULTS

Mineralogy

The BIF sample is composed of alternating massive dark grey Fe-oxide and white quartz layers (Fig. 2A). The millimetric Fe-oxide layers have a sharp contact with the quartz layer at the bottom and become gradually enriched in quartz (Fig. 2A). The Fe-oxide layers consist of martite crystals (~ 20 μm), which represent the hematitisation of euhedral magnetite (Fig. 2B). The pseudomorphic martite exhibits dissolution features along well-defined cleavage planes (Fig. 2C). The quartz layers are generally thicker than the Fe-oxide layers. Rare micrometric sized euhedral Ca-Mg and Ca-Fe carbonates, sulfides (galena, pyrite, chalcopyrite), and minor apatite, monazite and xenotime occur interstitial to, or form inclusions in quartz (Fig. 2D, E).

Biotite and grunerite of a few tens of micrometers, as well as kaolinite and illite are interstitial to the major minerals, quartz and hematite, and without any particular orientation.

Micrometric discontinuous Fe-oxide layers (Fig. 3A) occur mainly in the massive quartz layers and rarely at the interface of massive Fe-oxide and quartz layers. Fe-oxides infill cavities, which show negative crystal shapes of, presumably, dissolved minerals. These cavities are either walled by Fe-oxides and filled with spherulitic Fe-oxides (≤ 10 μm) (Fig. 3B, C), or they show no or partial Fe-oxide walls and are filled with Fe-oxides platelets or spherules (Fig. 3D,E). The latter are sometimes separated from the quartz by a nanometric (amorphous?) interface containing traces of Si, Al, Ca, Mn, Mg, P, Cu and S (Fig. 3E). At nanoscale, the spherules are composed of radially oriented fibers (Fig. 3F). Micro Raman spectroscopy indicates that the Fe-oxide spherules are hematite (Fig. 3G). FIB-TEM analyses of a Fe-oxide spherules (Fig. 4A-C) reveal a nanometric intergrowth of hematite and magnetite crystals (lattice parameters: 3.75 Å (012), 2.5 Å (110) and 2.3 Å (006) for hematite and 4.89 Å (11-1), 2.55 Å (311) and 2.97 Å (20-2) for magnetite), as shown on the Fast Fourier Transform (FFT) diffraction patterns. Carbon- and Fe-EDS mappings show C enrichments around the spherulitic Fe-oxide layers (Fig. 3C), also revealed by Raman mapping (deposit supplementary 1). Goethite needles are present on top of the Fe-oxide spherules (Fig. 3F)

Three type occurrences of CM were defined on the basis of NRA, FIB-TEM and Raman spectroscopy: (i) intergrown in nanometric hematite (+ minor magnetite) spherules (CM1) (Fig. 4D,E); (ii) encapsulated in quartz (CM2) in the vicinity of the massive and micrometric Fe-oxide layers (Fig. 5); (iii) in the discontinuous Fe-oxide alignments (Fig. 3A), either surrounding the Fe-oxide spherules, or in cavities around large martite grains (CM3) (Fig. 3B, D). According to FIB-TEM-EELS-EDX analyses, CM1 contains traces of N and C and Fe particles (Fig. 4B, C). NRA results show low N values (900 ppm) and high N/C ratios (5.5×10^{-3}) for CM2, while CM3 is characterized by high N values (5000 to 9000 ppm).

Carbonaceous matter: UV Raman spectroscopy

Raman spectra were recorded on two of the type occurrences: carbonaceous matter disseminated in the quartz matrix (CM2), and in the quartz crystal cavities around hematite spherules and large hematite crystals (CM3) (Fig. 3C), deposit supplementary figure 1). Due to the nanometric size of the CM intergrown in the hematite spherules, it was impossible to collect Raman spectra from CM1. Spectra acquired with the 244 nm excitation wavelength of all CMs exhibit a strong band at ~ 1600 cm^{-1} and a broad, less intense band at ~ 1380 cm^{-1} - 1400 cm^{-1} sometimes split into two peaks (Fig. 6). The additional peaks observed at lower wave numbers in CM2 (a broad peak at ~ 880 cm^{-1}, well-defined peaks at ~ 1066 cm^{-1}, ~ 1158 cm^{-1} and ~ 1230 cm^{-1}) are attributed to the quartz matrix (quartz spectrum not shown here; Fig. 6A). The Raman spectrum from CM in cavities may show a slight shoulder on the G-band at ~ 1730 cm^{-1} (Fig. 6B). The typical Raman spectrum of CM exhibits several carbon bands, the most intense being the first order band peaking at ~ 1600 cm^{-1} (G-band) and ~ 1350 cm^{-1} (D-band; e.g. (Beny-Bassez and Rouzaud, 1985; Wopenka and Pasteris, 1993; Ferrari and Robertson, 2000). The G-band (G for graphite) is assigned to the E_{2g2} vibrational mode of the aromatic plane and is present in all CM whatever the degree of structural order. On the other hand, the D-band (D for defects) is not present in perfectly stacked graphite and is induced by structural defects in the material. Therefore, these first-order carbon bands can be used to trace the CM maturity.

In order to interpret the UV Raman spectra in terms of maturation grade, a series of coal and kerogen standards were studied for comparison. The maturity of these standards was well known, and quantified by the mean maximum vitrinite reflectance (VR), determined according to the international standard ASTM D2798, on indigenous vitrinite macerals in coals, and in allochtonous vitrinites in type II kerogens. In this paper, VR (expressed in VR %) is the maturity indicator used for comparison with the Raman data. The results of Raman spectra

decomposition for the G and D bands are given in Table 2. Different Raman parameters such as peak position, peak intensity, full width at half maximum (FWHM), intensity ratios, Raman band separation, etc. can be used as maturity tracers depending on the maturity range (e.g. Beyssac et al., 2002; Kelemen and Fang, 2001; Quirico et al., 2005). In this study, the most sensitive tracers of maturity are the frequency spacing between G and D bands and the D-band position which both correlate with VR (Fig. 7). They point out that CM2 in quartz has a higher maturity (~ semi-anthracite) than CM3 from cavities. We can tentatively derive an "equivalent vitrinite reflectance" (eq-VR) indicator: a low maturity (eq-VR in the range 0.7-1.8 %) for CM3 in the crystal cavities, and a higher maturity range (eq-VR in the range 2.1-3.4 %) for CM2 disseminated in quartz, although no quantitative estimations can be taken from these plots (Fig. 7A, B). The higher maturity of CM2 encapsulated in quartz vs. CM3 in the cavities is revealed by micro Raman spectroscopy, and agrees with the lower N content in CM2 than in CM3 (900 ppm compared to 4000-9000 ppm, determined by NRA).

C-isotope geochemistry

The $\delta^{13}C$ analyses were carried out on separated Fe-oxide and quartz layers (Table 1). The quartz layers show lower $\delta^{13}C$ compositions ($\delta^{13}C$ = -24.7 to -20.8 ± 0.2 ‰) compared to the Fe-oxide layers (-21.8 to -19.4 ± 0.2 ‰). A bulk analysis of the sample is characterized by a $\delta^{13}C$ of -24.0 ± 0.2 ‰ (Table 1). The $\delta^{13}C$ values are not specific to individual CM phases (CM1 to CM3).

DISCUSSION

Origin of the Fe-oxide spherules

The BIFs of Bababudan Group are exposed to a tropical climate and in the first order weathering could be responsible for the Fe-oxide spherule formation (Muller, 1987). Evidence for supergene alteration of the Indian BIFs are: 1) goethite needles on top of the Fe-oxide spherules; 2) kaolinite interstitial to quartz and 3) immature organic matter (CM3; eq-VR ~ 1%) with high N contents (5000-9000 ppm) surrounding the Fe-oxide spherules, platelets or large former magnetite crystals in the cavities. Micrometric fissures around these cavities may have served as fluid pathways. However, weathering would have formed Fe-hydroxide spherules rather than radial Fe-oxide spherules composed of nanometric intergrown hematite and magnetite (Muller, 1987; Cornell and Schwertmann, 2003). Therefore a modern weathering process for the spherule formation is discarded.

The Fe-oxide spherules are hosted mainly in cavities forming micro layers within quartz bands, and at the interface of massive Fe-oxide and quartz layers. The shape of the cavities suggests the previous presences of dissolved minerals, and are thus negative crystal shapes of the former interstitial precipitates, which were probably carbonates, sulfides or phosphates since these minerals are rarely present. The chemical composition (Si, Al, Ca, Mn, Mg, P, Cu and S) of the amorphous (?) material at the interface between the quartz cavity wall and the hematite spherules (Fig. 3E) can thus be inherited from these precursor minerals. The fine radial texture of the spherules support crystallization in a cavity (e.g. Craig, 1981). Such radial textures resemble those formed during hydrothermal experiments at 150 °C – 200 °C in supersaturated solutions (model c and cf. figure 2j in Golden et al., 2008). Indeed, a large-scale hydrothermal event was recorded in the Chitradurga greenstone belt in the Western Dhawar craton, which is responsible for gold mineralisation at Gadag in the North (2.522 Ga) and Ajjanahalli in the south (2.520 Ga; Sarma et al., 2011). This event may be responsible for the spherule formation.

Spherulitic Fe-oxyhydroxides can form in the presence and/or absence of organic matter. Biomineralisation produces organized crystal chains and alignments (controlled biomineralisation; Kopp et al., 2004; Fortin and Langley, 2005) or irregular cell coatings and incrustations of heterogeneous Fe-oxide particles on bacteria (induced biomineralisation; Fortin and Langley, 2005; Frankel and Bazylinski, 2003, Toner at al. 2009; Gloter et al. 2004, Kennedy et al. 2004). Kappler and Newman (2004) described extra-cellular, poorly crystalline spherulitic Fe-(hydroxy) phosphates with smooth surfaces and rod-like internal nanostructures, but explained it by an abiotic mechanism as the result of Fe-sulfides dissolution. Fe-oxide spherules from hydrothermal environments may contain up to 18 wt.% CM (Halbach, 1986; Schwertmann et al., 1968) and biophilic elements (P, N, Mn, Si, S, Ca, Mg of up to 8 % of the total weight ; Tipping et al., 1981). Similar features, such as the presence of CM and biophilic elements, were observed for the here studied spherules, and therefore an interrelationship of Fe-oxide spherule formation and carbonaceous matter is likely. In low temperature hydrothermal solutions, spherical Fe-oxide particles can form by Fischer-Tropsch-Type (FTT) synthesis of carbonaceous matter (Yu et al., 2010). FFT CM can also be catalyzed by hematite and magnetite, but is however characterized by very low $\delta^{13}C$ values of -30 to -50 ‰ (McCollom and Seewald, 2006; Horita and Berndt, 1999; Sherwood Lollar, 2002), much lower than the here observed $\delta^{13}C$ of -24.7 to -19.4 ‰ ± 0.2 ‰. Thermal decarbonation of carbonates can produce carbonaceous matter with $\delta^{13}C$ values similar to those observed here (van Zuilen et al. 2003). This process requires higher temperatures (460-600°C at 5kb, van Zuilen et al. 2003) than determined for the Indian samples which experienced reducing greenschist facies conditions shown by the paragenesis of grunerite + biotite + quartz + magnetite in the studied samples.

However, the Indian BIFs are underlain by organic-carbon bearing phyllites (former black shales) with $\delta^{13}C$ values of -31.5 to -25.8 ‰, values that were attributed to denitrifying bacteria

(Kumar and Das Sharma, 1998). These values are only slightly lower than those of the overlying BIFs and therefore it is likely that the $\delta^{13}C$ isotopic composition of the CM in BIFs is related to the same biotic origin as for the CM in the phyllites. The lower $\delta^{13}C$ values in the BIFs compared to those in the phyllites might be related to the presence of CM3 and the more oxidizing conditions.

Preservation of organic matter

The preservation of carbonaceous matter in an oxidizing environment is related to its sorption onto magnetite-hematite surfaces (Mayer et al., 2004; Zimmerman et al., 2004; Salmon et al., 2000). The CM2 hosted in quartz, has low N contents and low N/C ratios (~ 5.5 x 10^{-3}). Such ratios are in the range of those obtained on separates from quartz of the same sample by step-heating extraction of N and C at high temperature (> 400 °C, N/C 1.4 x 10^{-1} to 4 x 10^{-4}, Hashizume, pers. comm., Hashizume et al., 2009). "Free" organic matter is released at lower temperatures than organic matter occluded in minerals (Pinti et al., 2007). The same analyses were carried out on the massive Fe-oxide layers giving the same low N/C ratios as in the quartz layers (Hashizume et al., 2009). Therefore the step-heating experiments reflect most likely the composition of CM1 occluded in the oxides. A semi anthracite-maturity (eq-VR = 2.1 – 3.4 %) was inferred from Raman spectrometry for CM2. From the above arguments, it can be concluded that CM1 and CM2 have the same degree of maturity, as heteroatoms such as N are known to be expelled during CM evolution (Tuinstra, 1970), and were formed and incorporated at the same time. Although similar low N/C-ratios as observed here are known from organic matter in Archean cherts (Pinti et al. 2001), semi-anthracite matury can also be reached by hydrothermal fluid influence (Ader et al. 2006). In the studied case hydrothermalism occurred at about 2.52 Ga (Sarma et al. 2011). At this stage of the study, it cannot be decided whether the organic matter was incorporated at the time of BIF

formation at 2.9 Ga or whether hydrothermal fluids transported organic matter from the underlying phyllitised black shales. A post-hydrothermal carbonaceous matter (CM1, CM2) infiltration into the BIFs would have produced larger CM agglomeration located at grain boundaries or in veinlets, or large aggregates in cavities as observed in black cherts from the Barberton greenstone belt (van Zuilen et al., 2007), or here, as the immature CM3. The iron particles observed in CM1 intergrown in the Fe-oxide spherules (Fig. 4D) may indicate a partial remineralization process. Such process is known from hydrothermal environments (Kerguelen Plateau and iron fertilizing experiments; Jacquet et al., 2008).

Conclusion

1. The Indian BIFs precipitated from an Fe-rich hydrothermal source. During diagenesis, alternating quartz and magnetite layers, and micrometric alignments or interstitial grains of Ca-, Mg-, Fe-carbonates, and locally, Fe-, Pb-, Cu-sulfides inclusions in quartz, were formed (Fig. 2A; Fig. 8A).

2. During the regional metamorphism (~ 2.6 Ga), diagenetic quartz and magnetite formed annealed textures, producing grunerite through carbonate dissolution (Fig. 8B).

3. The Fe-oxide spherules were formed in cavities, which represent the negative crystal shapes of previously dissolved carbonates or sulfides (Fig; 8C). The spherule formation occurred under hydrothermal conditions between 150 and 200°C, and may be related to the hydrothermal event recorded at 2.52 Ga in the Chitradurga Group which was responsible for the emplacement of the gold reefs.

4. The carbonaceous matters (CM1, 2 and 3) are of organic origin. The origin of CM1 and CM2 is attributed to an Archean event. On the basis of these results, it cannot be decided whether CM1 and CM2 were incorporated at the time of banded iron formation and diagenesis, or whether it were transported by the hydrothermal fluids from the underlying phyllites.

5. Hematitisation of the magnetite in the massive oxide layers increased the porosity. This increased porosity and permeability favored late fluid percolation and transport of CM3 and the formation of goethite and kaolinite during weathering.

6. Fe-oxides on the Martian surface should be investigated for carbonaceous matter as a possible biomarker.

Acknowledgments

This project was funded by the national PNP Planétologie, PRES UNIVERSUD Planétologie and the UMR IDES 8148 (CNRS-UPS). It is part of the ESF project 'Early Habitats of Early life'. Field-work in southern India was partially supported by a DST funded project to M. Jayananda. The authors thank Luce Delabesse, Valérie Godard and Madeleine Lenoble for technical help. Fabiana Ribeiro Dottori is thanked for the preparation of the samples for $\delta^{13}C$ analyses and logistic help. Rachael Morgan reviewed the manuscript for English.

REFERENCES

Ader, M., Cartigny, P., Boudou, J.P., Oh, J.H., Petit, E., Javoy, M. 2006. Nitrogen isotopic evolution of carbonaceous matter during metamorphism: methodology and preliminary results. Chemical geology. 232, 152-169.

Ahn, J.H. and Buseck, P.R., 1990. Hematite Nanospheres of Possible Colloidal Origin from a Precambrian Banded Iron Formation. Science, 250, 111-113.

Anil Kumar, A., Bhaskar Rao, Y.J., Sivaraman, T.V. and Gopalan, K., 1996. Sm–Nd ages of Archaean metavolcanics of the Dharwar craton, South India. Precambrian Research, 80, 205-216.

Beitler-Bowen, B., Benison, K.C., Oboh-Ikuenobe, F.E., Story, S. and Mormile, M.R., 2008.. Active hematite concretion formation in modern acid saline lake sediments, Lake Brown, Western Australia. Earth and Planetary Science Letters, 268, 52-63.

Beny-Bassez, C. and Rouzaud, J.N., 1985. Characterization of Carbonaceous Materials by Correlated Electron and Optical Microscopy and Raman Microspectroscopy. Scanning Electron Microscopy, 119-132.

Beyssac, O., Goffé, B., Petitet, J.-P., Froigneux, E., Moreau, M., Rouzaud, J.-N., 2003. On the characterization of disordered and heterogeneous carbonaceous materials by Raman spectroscopy. Spectrochimica Acta, Part A59, 2267-2276.

Brasier, M., McLoughlin, N., Green O. and Wacey, D., 2006. A fresh look at the fossil evidence for early Archaean cellular life. Philosophical Transactions of the Royal Society B-Biological Sciences, 361, 887-902.

Chadwick, B., Vasudev, V.N. and Hegde, G.V., 2000. The Dharwar craton, southern India, interpreted as the result of late Archaean oblique convergence. Precambrian Research, 99, 91-111.

Chan, M. A., Beitler, B., Parry, W. T., Ormo, J., Komatsu, G., 2004. A possible terrestrial analogue for haematite concretions on Mars. Nature. 429**,** 731-734.

Chardon, D., Jayananda, M., Chetty, T.R.K., Peucat, J-J., 2008, Precambrian continental strain and shear zone patterns: the South Indian case. J. Geophys. Res., 113, B08402, doi:10.1029/2007JB005299.

Chardon, D., Choukroune, P., Jayananda, M., 1996. Strain patterns, d´ecollement and incipient sagducted greenstone terrains in the Archaean Dharwar craton (south India). J. Struct. Geol. 18, 991–1004.

Christensen, P. R., Bandfield, J. L., Clark, R. N., Edgett, K. S., Hamilton, V. E., Hoefen, T., Kieffer, H. H., Kuzmin, R. O., Lane, M. D., Malin, M. C., Morris, R. V., Pearl, J. C., Pearson, R. Roush, T. L., Ruff, S. W., Smith, M. D., 2000. Detection of crystalline hematite mineralization on Mars by the Thermal Emission Spectrometer: Evidence for near-surface water. Journal of Geophysical Research-Planets. 105**,** 9623-9642.

Christensen, P. R., Bandfield, J. L., Hamilton, V. E., Ruff, S. W., Kieffer, H. H., Titus, T. N., Malin, M. C., Morris, R. V., Lane, M. D., Clark, R. L., Jakosky, B. M., Mellon, M. T., Pearl, J. C., Conrath, B. J., Smith, M. D., Clancy, R. T., Kuzmin, R. O., Roush, T., Mehall, G. L., Gorelick, N., Bender, K., Murray, K., Dason, S., Greene, E., Silverman, S., Greenfield, M., 2001. Mars Global Surveyor Thermal Emission Spectrometer experiment: Investigation description and surface science results. Journal of Geophysical Research-Planets. 106**,** 23823-23871.

Cornell, R. M. and Schwertmann, U. (2003) The Iron Oxides: Structure, Properties, Reactions, Occurrences and Uses. 664 p. Wiley-VCH.

Craig Jr, Vaughan, D.J., 1994. *Ore Microscopy and ore petrography,* John Wiley & sons. pp. 424.

Daudin, L.K. and Gallien, J.P., 2003. Development of "position-charge-time" tagged spectrometry for ion beam microanalysis. Nuclear Instruments and Methods in Physics Research Section B: Beam Interactions with Materials and Atoms, 210, 153-158.

Douglas, S., Abbey, W., Mielke, R., Conrad, P. and Kanik, I., 2008. Textural and mineralogical biosignatures in an unusual microbialite from Death Valley, California. Icarus, 193, 620-636.

Ferrari, A.C. and Robertson, J., 2000. Raman signature of bonding and disorder in carbons. Amorphous and Nanostructured Carbon. 593, 299-304.

Ferris, F.G.K., Lyven, B. and Pedersen, K., 1999. Accumulation of metals by bacteriogenic iron oxides in a subterranean environment. Geomicrobiology Journal, 16, 181-192.

Fortin D.F.G., 1998. Precipitation of iron, silica, and sulfate on bacterial cell surfaces. Geomicrobiology Journal, 15, 309-324.

Fortin, D. and Langley, S., 2005. Formation and occurrence of biogenic iron-rich minerals. Earth Science Reviews. 72, 1-19.

Frankel, R.B. and Bazylinski, D.A., 2003. Biologically induced mineralization by bacteria. Biomineralization. 54, 95-114.

Gloter, A., Zbinden, M., Guyot, F., Gaill, F., Colliex, C., 2004. TEM-EELS study of natural ferrihydrite fromgeological–biological interactions in hydrothermal systems. Earth and

Planetary Science Letters 222, 947– 957

Gnaneshwar Rao, T. and Naqvi S.M., 1995. Geochemistry, depositional environment and tectonic setting of the BIF's of the Late Archaean Chitradurga Schist Belt, India. Chemical Geology, 121, 217-243.

Golden D.C., Ming D.W., Morris R.V. and Graff T.G., 2008. Hydrothermal synthesis of hematite spherules and jarosite: Implications for diagenesis and hematite spherule formation in sulfate outcrops at Meridiani Planum, Mars. American Mineralogist, 93, 1201-1214.

Halbach, P., 1986. Processes Controlling the Heavy-Metal Distribution in Pacific Ferromanganese Nodules and Crusts. Geologische Rundschau, 75, 235-247.

Hashizume, K., Soyama, H., Cloquet, C., Pinti, D. L., Rouchon, V., Orberger, B., and Jayananda, M., 2008. Covariation of nitrogen and iron isotopic ratios in a banded iron formation. Geochimica Cosmochimica Acta, 72, A356-A356.

Hashizume, K., Soyama, H., Cloquet, C., Pinti, D.L., Rouchon, V., Orberger, B., and Jayananda, M., 2009. Inter-band variations of nitrogen, iron and argon-isotopic composition observed in a 2.9 Ga Indian BIF. Precambrian World Symposium; Fukuoka, Kyushu, Japan, 6^{th}-8^{th} March. A, p.50.

Horita, J. and Berndt, M.E., 1999. Abiogenic methane formation and isotopic fractionation under hydrothermal conditions. Science. 285, 1055-1057.

Jaquet, S.H.M., Dehairs, F., Savoye, N., Obernosterer, I., Christaki, U., Monnin, C., and Cardinal, D. (2008) Mesopelagic organic carbon remineralization in the Kerguelen Plateau region tracked by biogenic particulate Ba. Deep-Sea Research II, 55, 868-879.

Jayananda, M., Chardon, D., Peucat, J.J. and Capdevila, R., 2006. 2.61 Ga potassic granites and crustal reworking in the western Dharwar craton, southern India: tectonic, geochronological and geochemical constraints. Precambrian Research, 150, 1–26.

Jayananda, M., Banerjee, M., Pant, N.C., Dasgupta, S., Kano, T., Mahesha, N., Mahableswar, B., 2011. 2.62 Ga high-temperature metamorphism in the central part of the Eastern Dharwar Craton: implications for late Archaean tectonothermal history. Geol. Journal. DOI: 10.1002/gj.1308.

Kappler, A. and Newman D.K., 2004. Formation of Fe(III)-minerals by Fe(II)-oxidizing photoautotrophic bacteria. Geochimica et Cosmochimica Acta, 68, 1217-1226.

Kelemen, S.R. and Fang, H.L., 2001. Maturity trends in Raman spectra from kerofen and coal. Energy & Fuel, 15, 653-658.

Kennedy, C.B., Scott, S.D., Ferris, F.G. (2004). Hydrothermal phase stabilization of 2-line ferrihydrite by bacteria. Chemical Geology, 212, 269– 277.

Khodja, H., Berthoumieux, E., Daudin, L. and Gallien,J.P., 2001. The Pierre Süe Laboratory nuclear microprobe as a multi-disciplinary analysis tool. Nuclear Instruments and Methods in Physics Research Section B: Beam Interactions with Materials and Atoms, 181, 83-86.

Klein, C. and Beukes, N.J., 1992. Time distribution, stratigraphy, and sedimentologic settting, and geochemistry of Precambrian iron-formations. In J.C. Schopf, Ed., The Proterozoic Biosphere, p. 139-146. Cambridge University Press, Cambridge.

Klingelhöfer, G., Morris, R. V., Bernhardt, B., Schröder, C., Rodionov, D. S., de Souza Jr., P. A., Yen, A., Gellert, R., Evlanov, E. N., Zubkov, B., Foh, J., Bonnes, S. W., Arvidson, R. E., 2004. Jarosite and hematite at Meridiani Planum from Opportunity's Mossbauer spectrometer. Science. 306**,** 1740-1745.

Kolb, J.H., Rogers, A., Sinderen, S., Vennemann, T. Böttcher, M.E, and Meyer, F.M., 2004. The role of a transcrustal shear zone in orogenic gold mineralization at the Ajjanahalli mine, Dharwar craton, South India. Economic Geology, 99, 743-759.

Kopp, R.E., Nash, C.Z., Kirschvink, J.L. and Leadbetter, J.R., 2004. A possible magnetite/maghemite electrochemical battery in the magnetotatic bacteria. EOS, 85, GP34A-06.

Kumar, B. and Das Sharma, S., 1998. Carbon isotope systematics of graphites from Dharwar craton, southern India: implications to their source and post-depositional alterations. Current Science, 75. 4, 396-397.

Mayer, L.M., Schick, L.L., Hardy K.R., Wagai, R. and McCarthy, J. , 2004. Organic matter in small mesopores in sediments and soils. Geochimica et Cosmochimica Acta, 68, 3863-3872.

McCollom, T.M. and Seewald, J.S., 2006. Carbon isotope composition of organic compounds produced by abiotic synthesis under hydrothermal conditions. Earth and Planetary Science Letters. 243, 74-84.

McConchie, D., 1987. The geology and geochemistry of the Joffre and Whaleback shale members of the Brockman Iron Formation, Western Australia. In P. Appel and G.L. Laberge, Eds., Precambrian Iron-Formations, p. 541-597. Theophastus, Athens.

McLennan, S. M., Bell Iii, J. F., Calvin, W. M., Christensen, P. R., Clark, B. C., de Souza, P. A., Farmer, J., Farrand, W. H., Fike, D. A., Gellert, R., Ghosh, A., Glotch, T. D., Grotzinger, J. P., Hahn, B., Herkenhoff, K. E., Hurowitz, J. A., Johnson, J. R., Johnson, S. S., Jolliff, B., Klingelhöfer, G., Knoll, A. H., Learner, Z., Malin, M. C., McSween, Jr H. Y., Pocock, J., Ruff, S. W., Soderblom, L. A., Squyres, S. W., Tosca, N. J., Watters, W. A., Wyatt, M. B., Yen, A., 2005. Provenance and diagenesis of the evaporite-bearing Burns formation, Meridiani Planum, Mars. Earth and Planetary Science Letters. 240**,** 95-121.

Morris, R. V., Klingelhofer, G., Schroder, C., Rodionov, D. S., Yen, A., Ming, D. W., de Souza, P. A., Wdowiak, T., Fleischer, I., Gellert, R., Bernhardt, B., Bonnes, U., Cohen, B. A., Evlanov, E. N., Foh, J., Gutlich, P., Kankeleit, E., McCoy, T., Mittlefehldt, D. W., Renz, F., Schmidt, M. E., Zubkov, B., Squyres, S. W., Arvidson, R. E., 2006. Mossbauer mineralogy of rock, soil, and dust at Meridiani Planum, Mars: Opportunity's journey across sulfate-rich outcrop, basaltic sand and dust, and hematite lag deposits. Journal of Geophysical Research-Planets. 111.

Muller, J.P., 1987. Analyse pétrologique d'une formation latéritique meuble du Cameroun. PhD thesis, Université Paris VII, Paris, France. 230pp.

Nutman, A.P., Chadwick, B., Krishna, R., and Vasudev, V.N., 1996. SHRIMP U-Pb Zircon ages of acid volcanic rocks in the Chitradurga and Sandur Groups and granites adjacent to Sandur Schist belt. Journal of the Geological Society of India, 47, 153-161.

Orberger, B., Rouchon, V., Westall. F., de Vries S.T., Pinti, D.L., Wagner, C., Wirth, R. and Hashizume, K., 2006. Microfacies and origin of some Archean cherts (Pilbara, Australia). Geological Society of America, 405, 133-156.

Orberger, B., Vymazalova, A., Wagner, C., Fialin, M., Gallien, J P, Wirth, R. Pasava, J. and Montagnac, G., 2007a. Biogenic origin of intergrown Mo-sulphide- and carbonaceous matter in Lower Cambrian black shales (Zunyi Formation, southern China). Chemical Geology, 238, 213-231.

Orberger, B., Wirth, R., Rividi, N., Wagner, C., Hofmann, A., Gallien, J. P., Montagnac, G., and Quirico, E., 2007b. Nanometric jarosite/alunite in carbonaceous matter rich cherts: Marble bar drill core (#1 ABDP): Indications for acid-sulfate conditions in a hydrothermal system. Geochimica et Cosmochimica Acta, 71, A742-A742.

Pasteris, J., 1989. In situ analysis in geological thin-sections by laser Raman microprobe spectroscopy. - a cautionary note. Applied Spectroscopy, 43, 567-570.

Pinti, D.L., Hashizume, K., and Matsuda, J., 2001. Nitrogen and argon signatures in 3.8 to 2.8

Ga metasediments: Clues on the chemical state of the Archean ocean and the deep biosphere: Geochimica et Cosmochimica Acta, v. 65, 2301–2315.

Pinti, D.L., Hashizume, K., Orberger, B. Gallien, J.P., Cloquet, C. and Massault, M., 2007. Biogenic nitrogen and carbon in Fe-Mn-oxyhydroxides from an Archean chert, Marble Bar, Western Australia. Geochemistry Geophysics Geosystems, 8. N2, 1-19.

Quirico, E., Rouzaud, J.N., Bonal, L. and Montagnac, G., 2005. Maturation grade of coals as revealed by Raman spectroscopy: Progress and problems. Spectrochimica Acta Part a-Molecular and Biomolecular Spectroscopy, 61, 2368-2377.

Quirico, E., Montagnac, G., Rouzaud, J.N., Bonal, L., Bourot-Denise, M., Duber, S. and Reynard, B., 2009. Precursor and metamorphic condition effects on Raman spectra of poorly ordered carbonaceous matter and coals. Earth and Planetary Science Letters, 287, 185-193.

Raith, M.R., Ackermand, D., and Lal, R.K., 1982. The Archaean craton of southern India: metamorphic evolution and P–T conditions. Geologische Rundschau, 71, 280-290.

Salmon, V., Derenne, S., Lallier-Vergès, E., Largeau, C. and Beaudoin, B. (2000) Protection of organic matter by mineral matrix in a Cenomanian black shale. Organic Geochemistry, 31, 463-474.

Schwertmann, U., Fischer, W.R., and Papendorf, H., 1968. The influence of organic compounds on the formation of iron oxides. In: 9th International Congress in Soil Sciences, Adelaide, Australia, 645-655.

Seshadri, T.S., Chauduri, P., Harinadha Babu, and Chayapathi, N., 1981. Early Precambrian Supracrustals of Southern Karnataka. Memoire of the Geological Society of India 112, 163-198.

Sherwood Lollar, B., 2002. Abiogenic formation of alkanes in the Earth's crust as a minor source for global hydrocarbon reservoirs. Nature. 416, 522-524.

Sarma, S.D., Fletcher, I.R., Rasmussen, B., McNaughton, N.J., Mohan, M.R., Groves, D.I., 2011. Archean gold mineralization synchronous with late cratonization of the Western Dhawar Craton, India: 2.52 Ga U-Pb ages of hydrothermal monazite and xenotime in gold deposits. Mineralium Deposita,46, 273-288.

Srinivasan, R. and Ojakangas, R.W., 1986. Sedimentology of quartz-pebble conglomerates and quartzites of the Archaean Bababudan Group, Dharwar Craton, South India: evidence for early crustal stability. Journal of the Geological Society of India, 94, 199-214.

Swami Nath, J., Ramakrishnan, M., Viswanatha, M.N., 1976. Dharwar stratigraphic model and Karnataka craton evolution. Geol. Surv. India record. 107,149-175.

Swaminath, J. and Ramakrishnan, M., 1981. Memoire of the Geological Society of India. 112, 5-38.

Taylor, P.N., Chadwick, B., Moorbath, S., Ramakrishanan, M. and Viswanatha, M.N., 1984. Petrography, chemistry and isotopic ages of Peninsular Gneisses, Dharwar, acid volcanics and Chitradurga granite with special reference to Archean evolution of Karnataka craton, Southern India, Precambrian Research 23 (3-4), 349-375.

Toner, B.M., Santelli, C.M., Marcus, M.A., Wirth, R., Chan, C.S., McCollom, T., Bach, W., Edwards, K.J., 2009a. Biogenic iron oxyhydroxide formation at mid-oceanridge hydrothermal vents: Juan de Fuca Ridge. gechimica et Cosmochimica Acta, 73, 388-403.

Tipping, E, Woof, C. and Cooke, D., 1981. Iron oxide from a seasonally anoxic lake. Geochimica et Cosmochimica Acta, 45, 1411-1419.

Trendall, A.F., De Laeter, J.R., Nelson, D.R. and Mukhopadhyay, D., 1997. A precise U–Pb age for the base of Mulaingiri formation (Bababudan Group, Dharwar Supergroup) of the Karnataka craton. Journal of the Geolological Society of India 50, 161–170.

Tuinstra F.A.K., 1970. Raman spectrum of graphite. Journal of Chemistry and Physics, 53, 1126-1130.

Tyler P.A. and Buckney R.T., 1980. Ferromanganese concretions in Tasmania lakes. Australian Journal of Marine and Freshwater Research, 31, 525-531.

Ueno, Y., Yoshioka, H., Maruyama, S. and Isozaki, Y., 2004. Carbon isotopes and petrography of kerogens in 3.5 Ga hydrothermal silica dikes in the North Pole area, Western Australia. Geochimica et Cosmochimica Acta, 68, 3, 573-589.

Van Zuilen, M.A., Lepland, A. and Arrhenius, G., 2002. Reassessing the evidence for the earliest traces of life. Nature, 420, 202-202.

Van Zuilen, M A., Lepland, A., Teranes, J., Finarelli, J., Wahlen, M. and Arrhenius, G. , 2003. Graphite and carbonates in the 3.8 Ga old Isua Supracrustal Belt, southern West Greenland. Precambrian Research, 126, 331-348.

Van Zuilen, M.A., Thomazo, C., Luais, B. and Philippot, P., 2007. Carbon and iron isotopic evidence for photosynthesis in a 3.5 Ga old shallow marine depositional environment. Geochimica et Cosmochimica Acta. 71, A1058-A1058.

Varajao, C.A.C., Bruand, A., Ramanadaidou, E.R. and Gilkes, R.J., 2002. Microporosity of BIF hosted massive hematite ore. Anais da Academia Brasileira de Ciencias, 74(1), 113-126.

Wirth, R., 2004. Focused Ion Beam (FIB): A novel technology for advanced application of micro- and nanoanalysis in geosciences and applied mineralogy. European Journal of Mineralogy, 16, 863-876.

Wopenka, B. and Pasteris, J. D., 1993. Structural Characterization of Kerogens to Granulite-Facies Graphite - Applicability of Raman Microprobe Spectroscopy. American Mineralogist. 78, 533-557.

Yoshioka H, Kumazawa M, Ohta K. and Handa N., 2001. Manganese micronodules containing organic matter in an archean banded-iron formation. In S. Nakashima, Ed., Geochemistry and the Origin of Life, p. 251-268. Universal Academy Press. Inc., Tokyo, Japan.

Yu, G., Sun, B., Pei, Y., Xie, S.,Yan, S., Qiao, M., Fan, K., Zhang, X. and Zong, B., 2010. FexOy@C Sphères as an excellent catalyst for Fischer-Tropsch Synthèses. Journal of the American Chememical Society, 132, 935-937.

Zhang, L, He, R., and Gu, H.C., 2006. Synthesis and kinetic shape and size evolution of magnetite nanoparticles. Materials Research Bulletin, 41, 260-267.

Zimmerman, A.R., Goyne, K.W., Chorover, J., Komarneni, S. and Brantley, S.I., 2004. Mineral mesopore effects on nitrogenous organic matter adsorption. Organic Geochemistry, 35, 355-375.

Zolotov, M. Y., Shock, E. L., 2005. Formation of jarosite-bearing deposits through aqueous oxidation of pyrite at Meridiani Planum, Mars. Geophysical Research Letters. 32. L21203, doi:10.1029/2005GL024253

Figure captions

Fig. 1A. Geological map of the Chitradurga basin, Dharwar Supergroup, (Dharwar Craton, Southern India) showing the sample location, (modified after Jayananda et al. 2006); **B.** Stratigraphic column of the Bababudan and Chitradurga groups, Dharwar Craton, India.

Fig. 2A. Thin section scan of BIF 14A showing the Fe-oxide layers (black) alternating with quartz layers (white). The quartz layers contain micrometric continuous or discontinuous Fe-oxide layers. The massive Fe-oxide layers gradually become richer in quartz layers. Backscattered scanning electron (BSE) microphotographs: **B.** Band of martitized magnetite in a quartz layer; **C.** Euhedral martitized magnetite showing dissolution features; **D**. Euhedral Ca-Fe-Mg carbonates interstitial to quartz in the massive quartz layers; **E.** Xenotime and monazite in quartz layers, and Fe and Cu sulfide inclusion in quartz grains;

Fig. 3A. Micrometric alignments in quartz layers composed of crystal cavities interstitial to quartz grains; a few martitized magnetite crystals occur. **B.** Close view (BSE image) of an oxide-bearing cavity from a micrometric alignment (Fig. 3A): Hematite walls the cavity, while the central part is composed of Fe-oxide spherules. **C.** EDX mapping of Fe and C of the cavity shown in Fig. 2. The Fe oxide spherules are embedded in CM (further quoted as CM3). BSE images: **D.** Hematite platelets filling cavities; **E.** Hematite spherules infilling a crystal cavity; they are separated from the host quartz wall by an amorphous interface hosting biophilic elements; **F.** Hematite spherules composed of radial oriented fibers. **G.** Raman spectrum of hematite (martitized magnetite) obtained with laser excitation at 514.5 nm.

Fig. 4 A. Focused ion beam cut through the Fe-oxide spherules. **B. and C:** left, High Resolution Transmission Electron Microscope photographs (HRTEM) of the Fe-oxide spherules and right, FFT diffraction pattern images of the marked areas indexing magnetite (mgt) and hematite (hem). The FFT diffraction pattern is given along the [1-21] axis for magnetite (B). **D**. TEM image and EDX mapping of carbonaceous matter CM1 intergrown in the Fe-oxide spherules. CM1 shows the presence of iron particles. **E.** Electron energy loss spectroscopy (EELS) of carbonaceous matter CM1, indicating traces of Ca and N.

Fig. 5. Nuclear reaction analyses of Fe-oxides showing C-rich spot (CM2) included in quartz at the interface with euhedral Fe-oxides. Enlarged EDX mappings of the C-rich spot reveal heterogeneous traces of N, K and Ca in CM2.

Fig. 6. Representative Raman spectra of carbonaceous matter: **A**. disseminated in the quartz matrix (CM2) and **B**. embedding the hematite spherules (CM3) obtained with laser excitation at 244 nm. The spectra show the carbon D and G first order bands and a few well-defined peaks attributed to the quartz matrix in (**A**).

Fig. 7. Results of spectra decomposition. Correlations of Raman parameters G-D band separation **(A)** and D band position **(B)** with the vitrinite reflectance (VR %) defined by a series of standard coals from the Penn State Coal Data Bank and type II kerogens provided by the Institut Français du Pétrole (Quirico et al., 2005). On both diagrams, the linear regression was established from the coal data, and the error bars are 2σ; the total set of data for the standards is available from the authors. For the studied CM2 and CM3 samples, the Y error bars (2σ) delimit the range of measured values (Table 2) and the X bars delimit the corresponding range of VR % values using the standard calibration curve.

Fig. 8A-D: Conceptual model explaining the different stages of BIF evolution from the depositional environment **(A)** to diagenesis **(B)**, metamorphism at ~2.6 Ga **(C)** to hydrothermalism at ~2.52 Ga and Fe-oxide spherule formation **(D)**.

Table captions

Table 1. Carbon isotopic composition (PDB normalized) of the individual Fe-oxide and quartz layers. Numbers correspond to the different layers in Fig. 2A. Total uncertainties on the measurement are of ± 0.2 ‰.

Table 2. Raman spectroscopy results for Indian carbonaceous matter (CM). pos G, pos D: G- and D-band position; Std: standard deviation; FWHM: full width at half maximum.

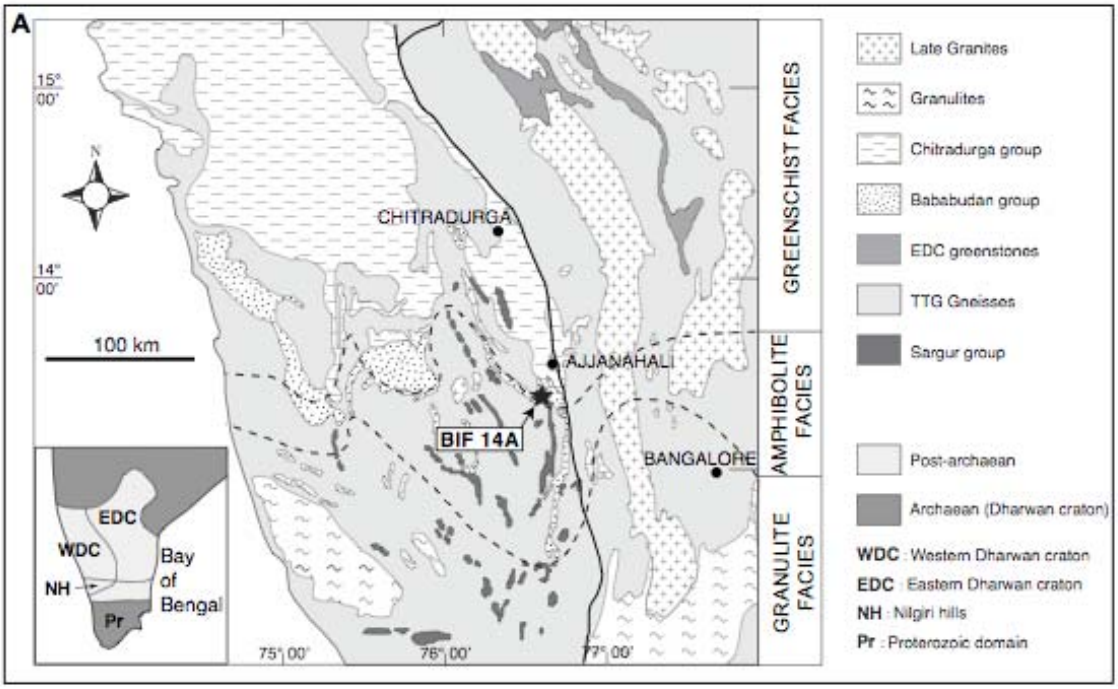
A
15° 00'
14° 00'
N
100 km
CHITRADURGA
AJJANAHALI
BIF 14A
BANGALORE
EDC
WDC
NH
Pr
Bay of Bengal
75° 00'
76° 00'
77° 00'
GREENSCHIST FACIES
AMPHIBOLITE FACIES
GRANULITE FACIES
Late Granites
Granulites
Chitradurga group
Bababudan group
EDC greenstones
TTG Gneisses
Sargur group
Post-archaean
Archaean (Dharwan craton)
WDC : Western Dharwan craton
EDC : Eastern Dharwan craton
NH : Nilgiri hills
Pr : Proterozoic domain

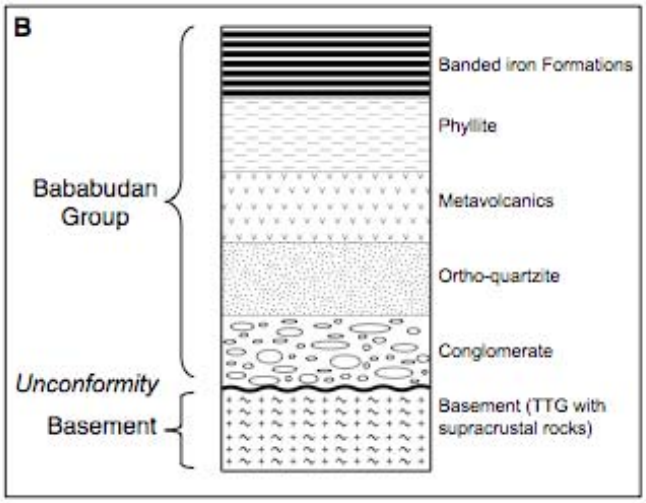
B
Banded iron Formations
Phyllite
Metavolcanics
Ortho-quartzite
Conglomerate
Bababudan Group
Unconformity
Basement
Basement (TTG with supracrustal rocks)

FIGURE 1 a+b

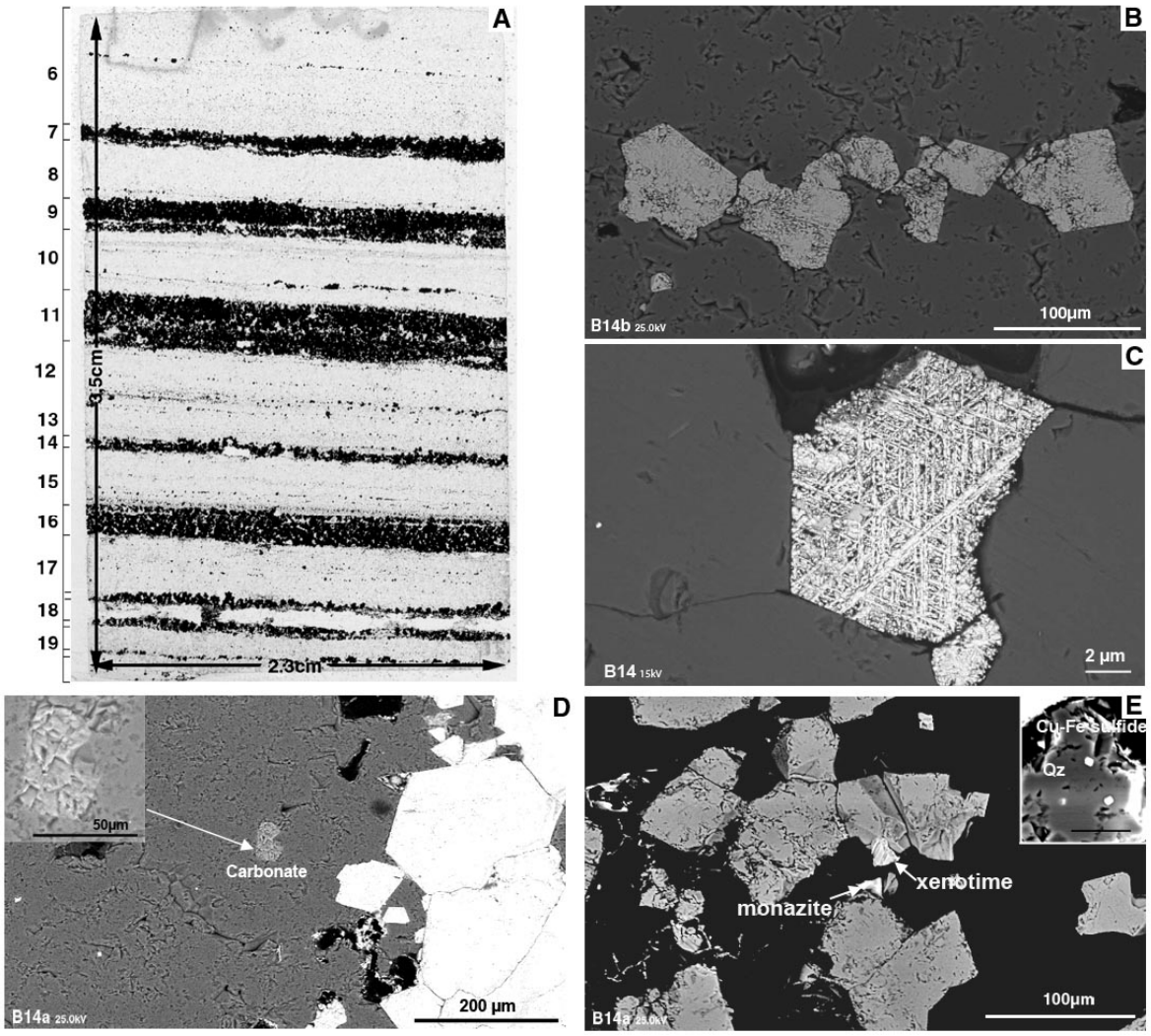
A
6
7
8
9
10
11
12
13
14
15
16
17
18
19
3.5cm
2.3cm
B
B14b 25.0kV
100µm
C
B14 15kV
2 µm
D
50µm
Carbonate
B14a 25.0kV
200 µm
E
Cu-Fe sulfide
Qz
xenotime
monazite
100µm

FIGURE 2A-E

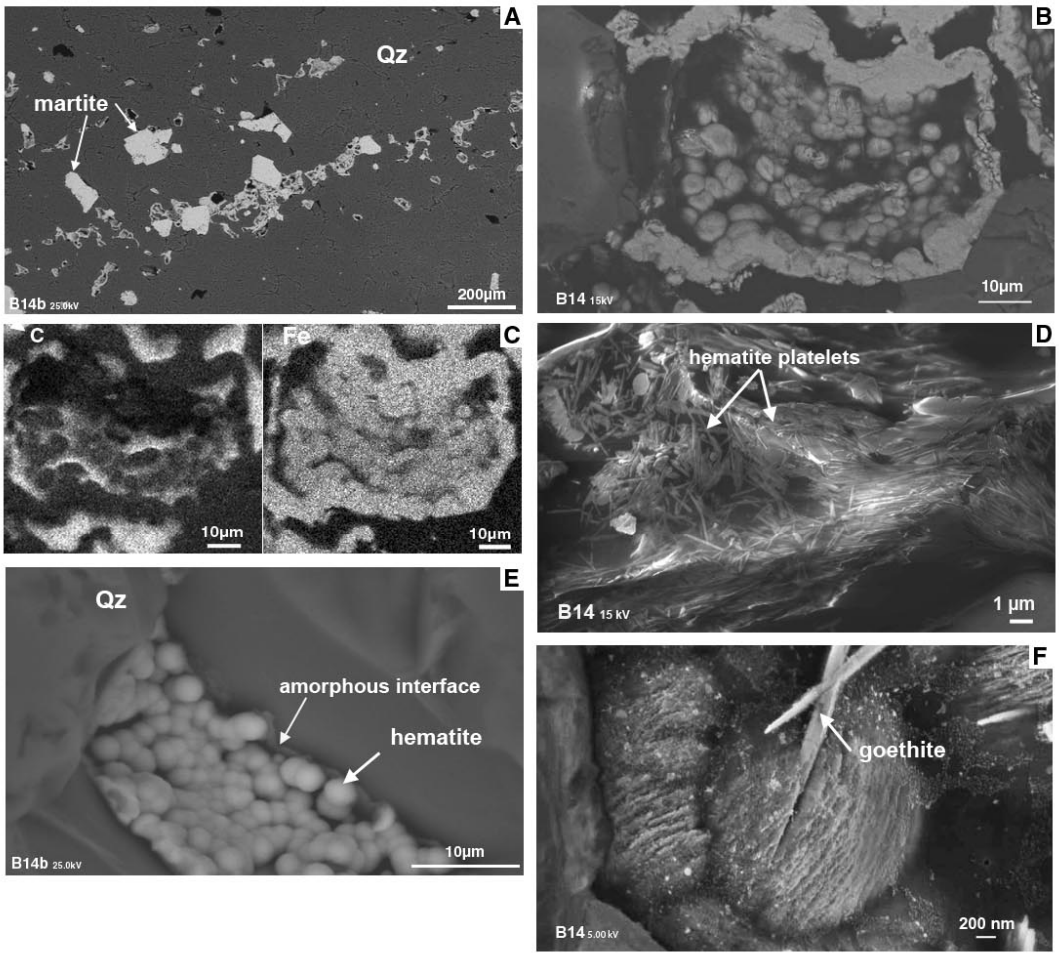

Fig.3

Figure 3 A-F

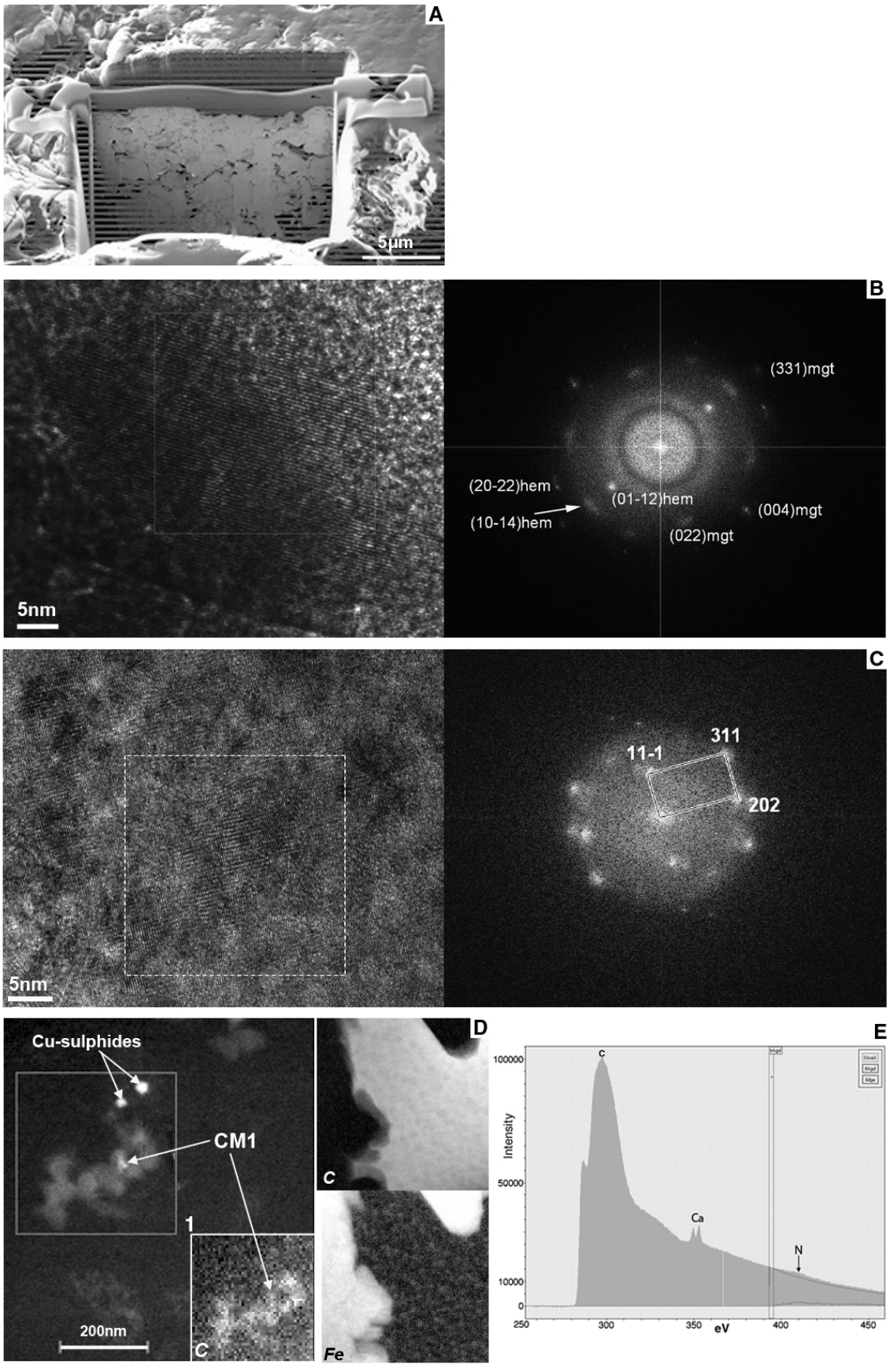
A
5µm
B
(331)mgt
(20-22)hem
(01-12)hem
(10-14)hem
(004)mgt
(022)mgt
5nm
C
311
11-1
202
5nm
Cu-sulphides
CM1
1
200nm
C
D
C
Fe
E
100000
50000
10000
0
Intensity
C
Ca
N
250
300
350
400
450
eV

Fig.4

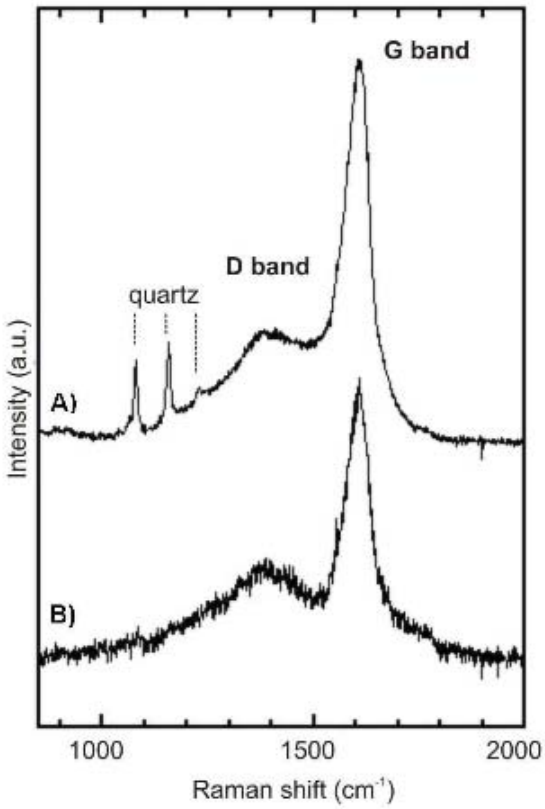
G band
D band
quartz
A)
B)
Intensity (a.u.)
1000
1500
2000
Raman shift (cm-1)

Figure 6

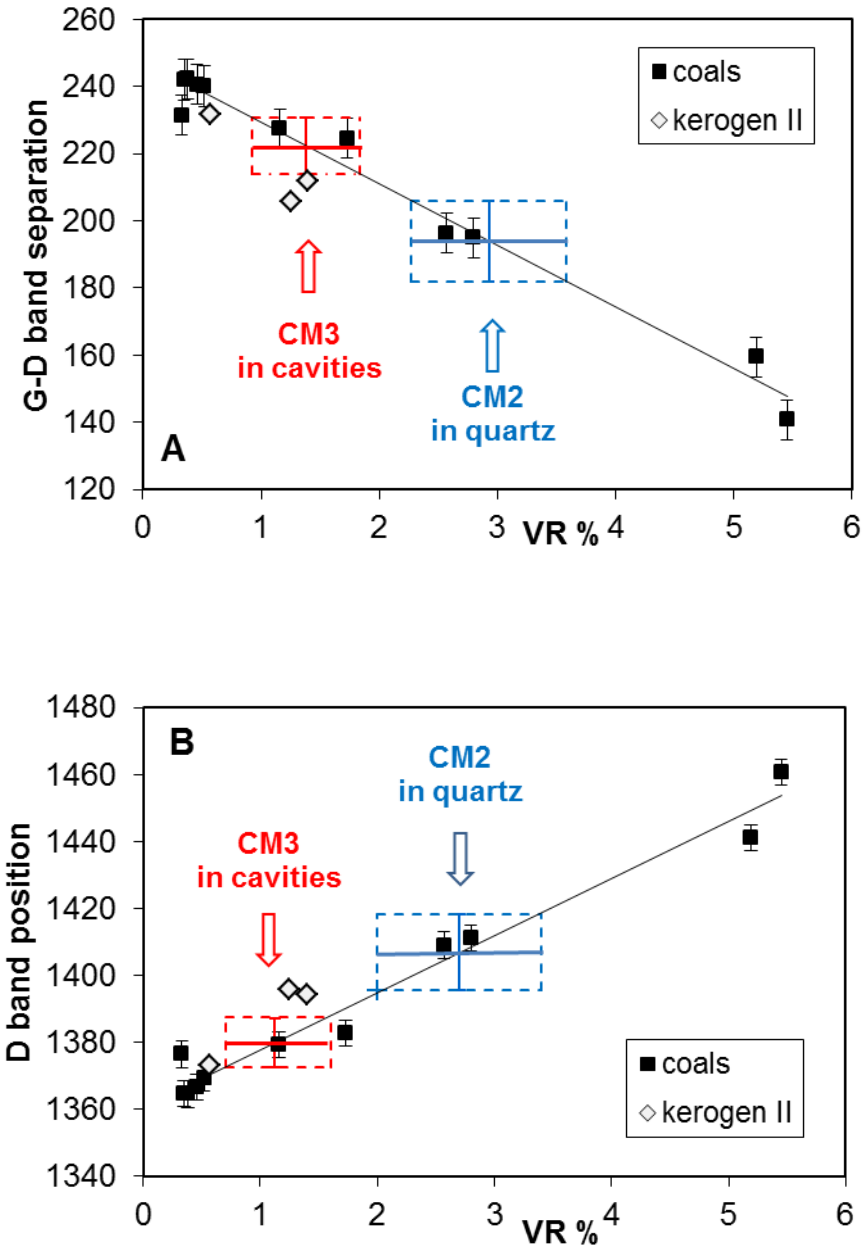
A
G-D band separation
VR %
coals
kerogen II
CM3
in cavities
CM2
in quartz
B
D band position
VR %
coals
kerogen II
CM3
in cavities
CM2
in quartz

FIGURE 7

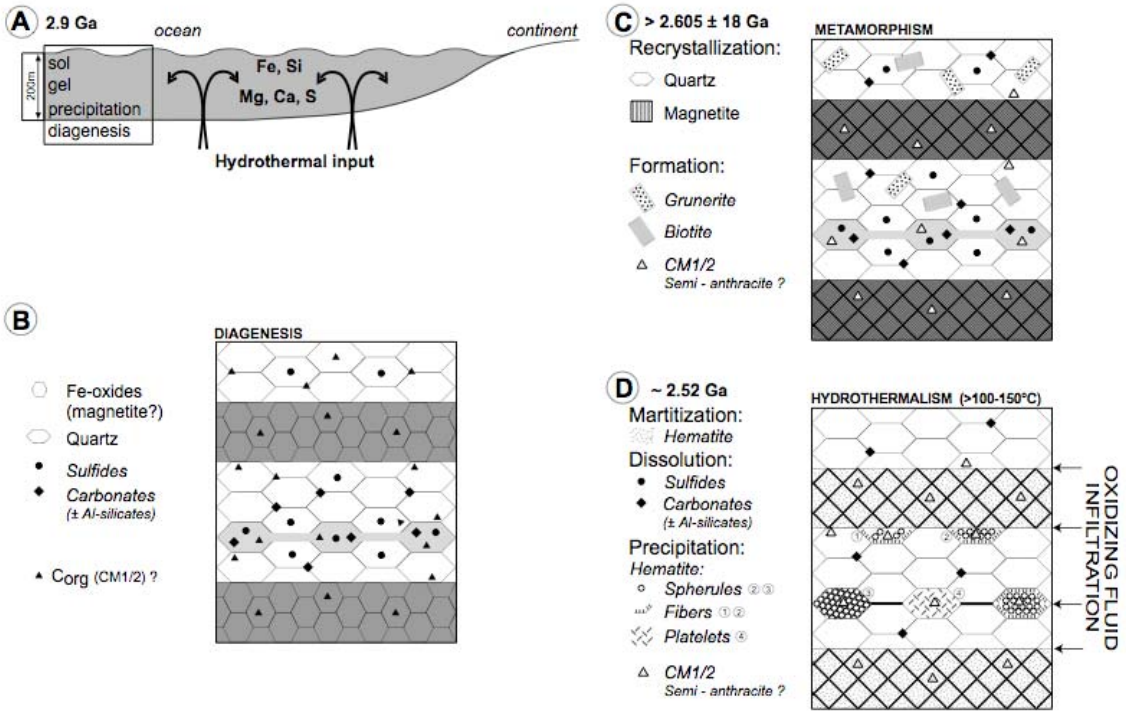
A
2.9 Ga
ocean
continent
200m
sol
gel
precipitation
diagenesis
Fe, Si
Mg, Ca, S
Hydrothermal input
B
DIAGENESIS
Fe-oxides
(magnetite?)
Quartz
Sulfides
Carbonates
(± Al-silicates)
Corg (CM1/2) ?
C
> 2.605 ± 18 Ga
Recrystallization:
Quartz
Magnetite
Formation:
Grunerite
Biotite
CM1/2
Semi - anthracite ?
METAMORPHISM
D
~ 2.52 Ga
Martitization:
Hematite
Dissolution:
Sulfides
Carbonates
(± Al-silicates)
Precipitation:
Hematite:
Spherules
Fibers
Platelets
CM1/2
Semi - anthracite ?
HYDROTHERMALISM (>100-150°C)
OXIDIZING FLUID
INFILTRATION

Figure 8

TABLE 1. $\delta^{13}C$ values (± 0.2 %).

#	layer	$\delta^{13}C$
6	quartz	-23.87
9	Fe-oxide	-21.75
10	quartz	-24.24
11	Fe-oxide	-19.37
12	quartz	-24.66
15	quartz	-24.47
16	Fe-oxide	-19.98
17	quartz	-24.01
18	quartz	-23.32
19	quartz	-20.77
26	Fe-oxide	-20.19
	bulk	-24.03

: number of the different layers
of Figure 2A, except #26 not shown.

TABLE 2. Raman spectroscopy results for Indian carbonaceous matter (CM)

	pos G (cm^{-1})	std	FWHM-G	std	pos D (cm^{-1})	std	FWHM-D	std	G-D separ.	std	area ratio	std
CM2	1600.7	2.4	75.6	17.7	1406.8	11.3	243.6	35.5	193.9	12	1.2	0.3
CM3	1602.3	1.9	75.5	5	1379.9	7.3	256	53.8	222.3	8.5	1	0.2

Average values and standard deviation (std) of 16 pectra for CM disseminated in the quartz matrix (CM2)
and 25 spectra for CM found in the spherule-bearing cavities and around large hematitized magnetite (CM3).
Pos: peak position of the G and D bands; FWHM: Full Width Half Maximum; G-D separ: G-D band separation.

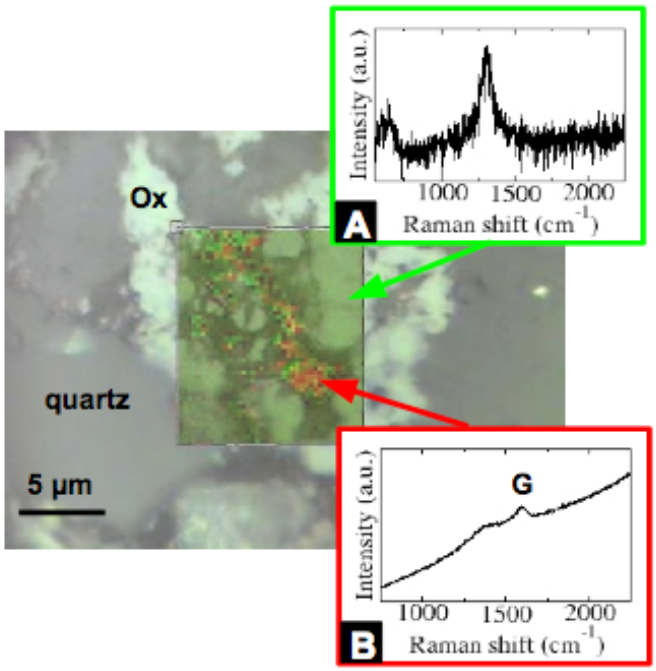

APPENDIX 1

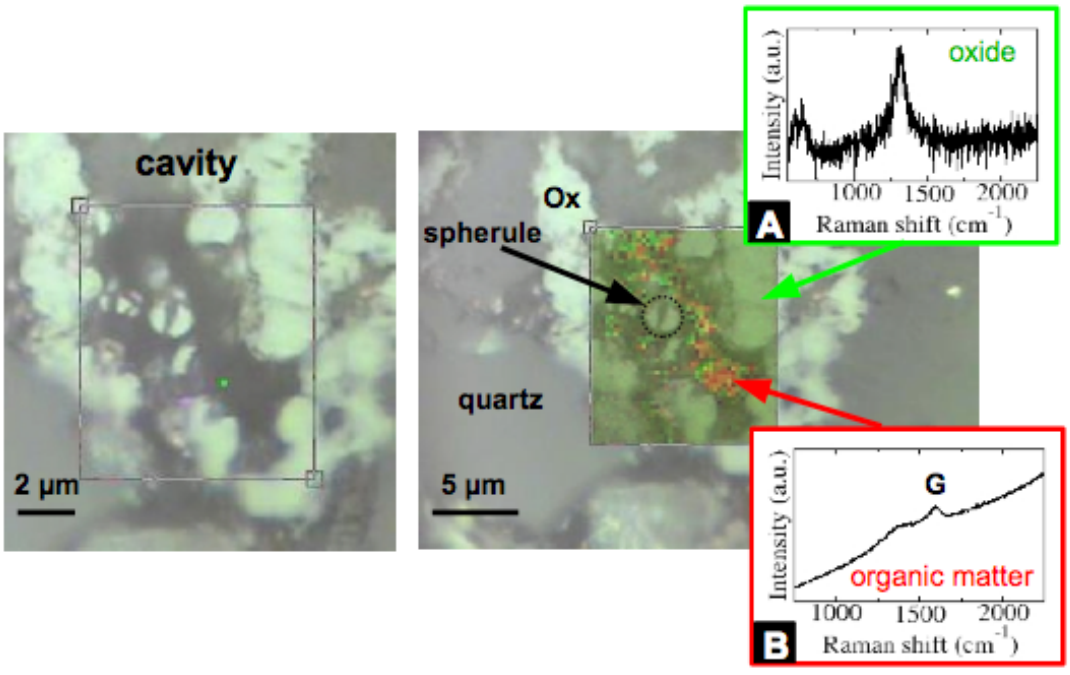

Deposit Item

Figures 1A+B

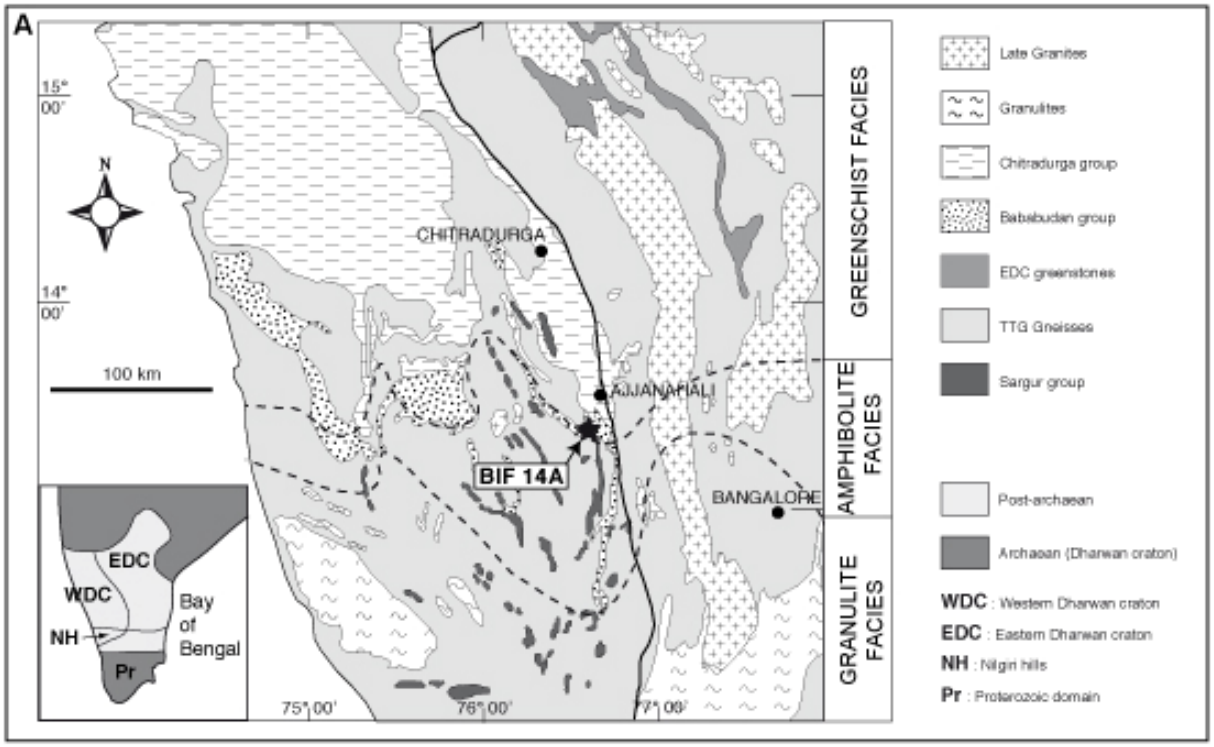
A
15° 00'
14° 00'
N
100 km
CHITRADURGA
AJJANAHALI
BIF 14A
BANGALORE
EDC
WDC
NH
Pr
Bay of Bengal
75° 00'
76° 00'
77° 00'
GREENSCHIST FACIES
AMPHIBOLITE FACIES
GRANULITE FACIES
Late Granites
Granulites
Chitradurga group
Bababudan group
EDC greenstones
TTG Gneisses
Sargur group
Post-archaean
Archaean (Dharwar craton)
WDC : Western Dharwar craton
EDC : Eastern Dharwar craton
NH : Nilgiri hills
Pr : Proterozoic domain

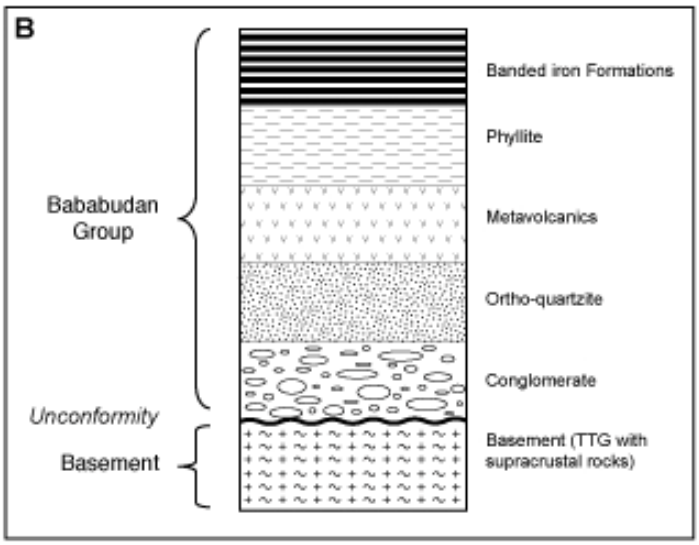
B
Bababudan Group
Unconformity
Basement
Banded iron Formations
Phyllite
Metavolcanics
Ortho-quartzite
Conglomerate
Basement (TTG with supracrustal rocks)

Figure 2

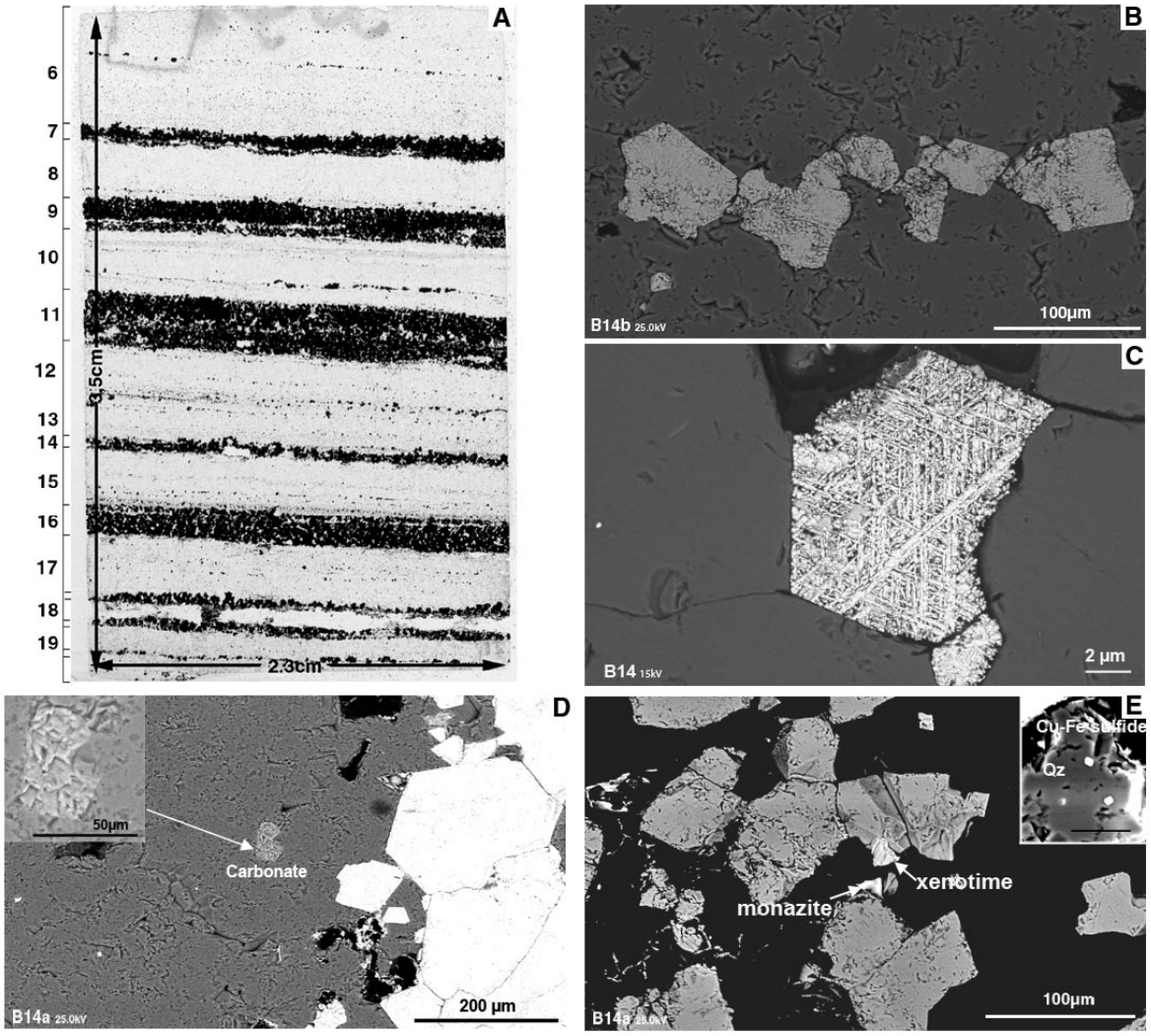
A
6
7
8
9
10
11
12
13
14
15
16
17
18
19
3.5cm
2.3cm
B
B14b 25.0kV
100µm
C
B14 15kV
2 µm
D
50µm
Carbonate
B14a 25.0kV
200 µm
E
Cu-Fe sulfide
Qz
xenotime
monazite
100µm

Figure 3

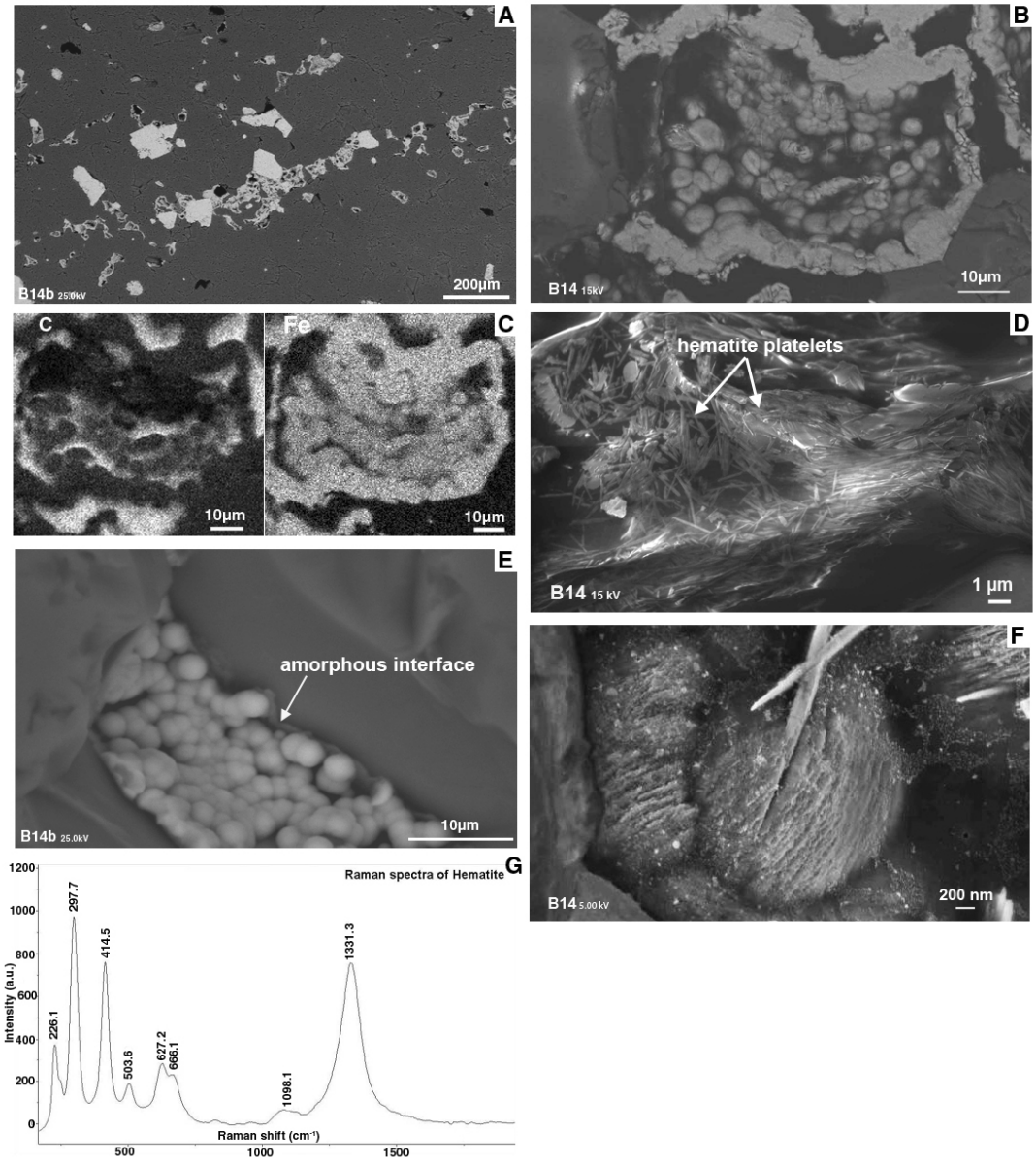

Fig.3

Figure 4

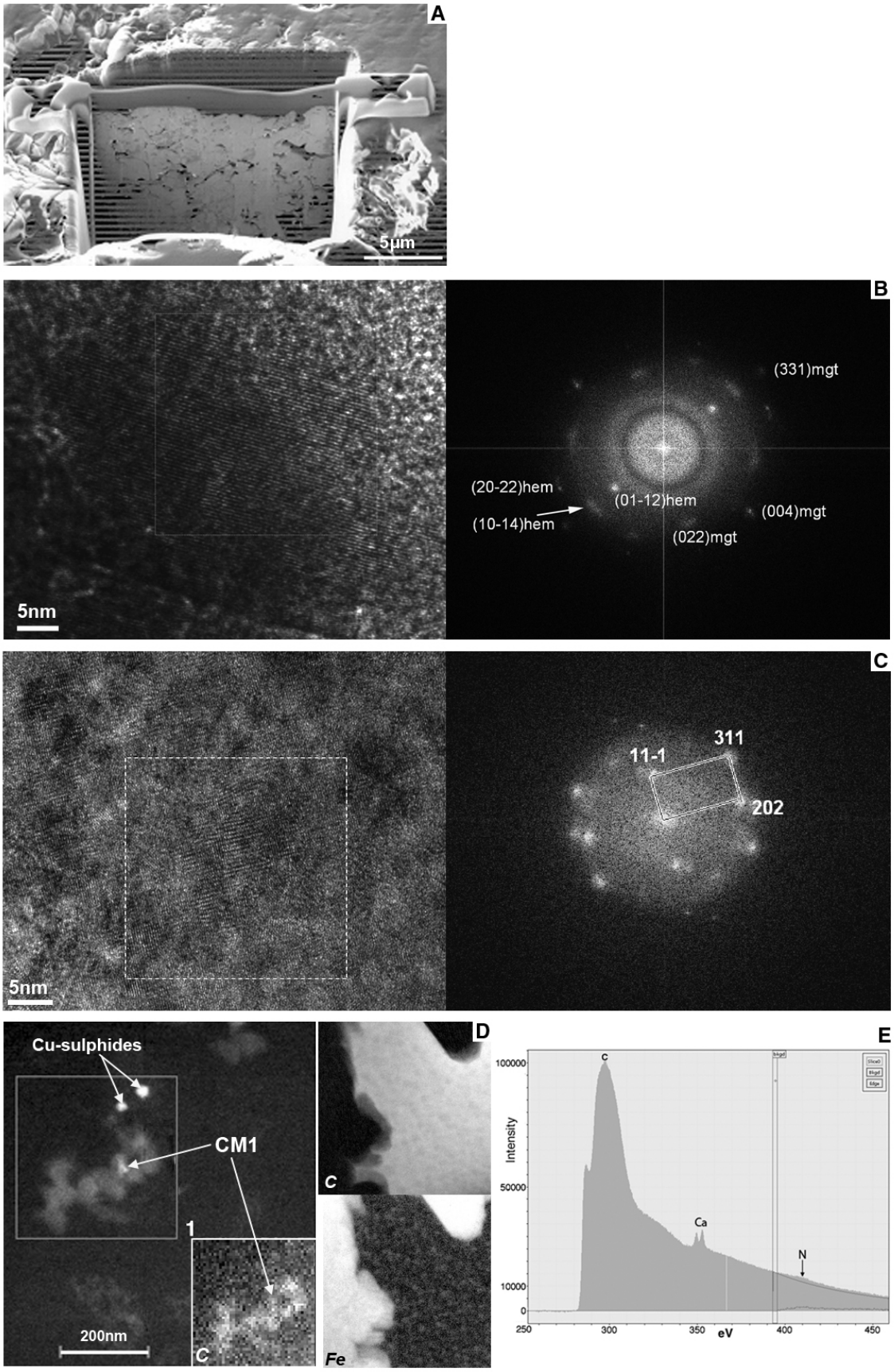

Fig.4

Figure 5

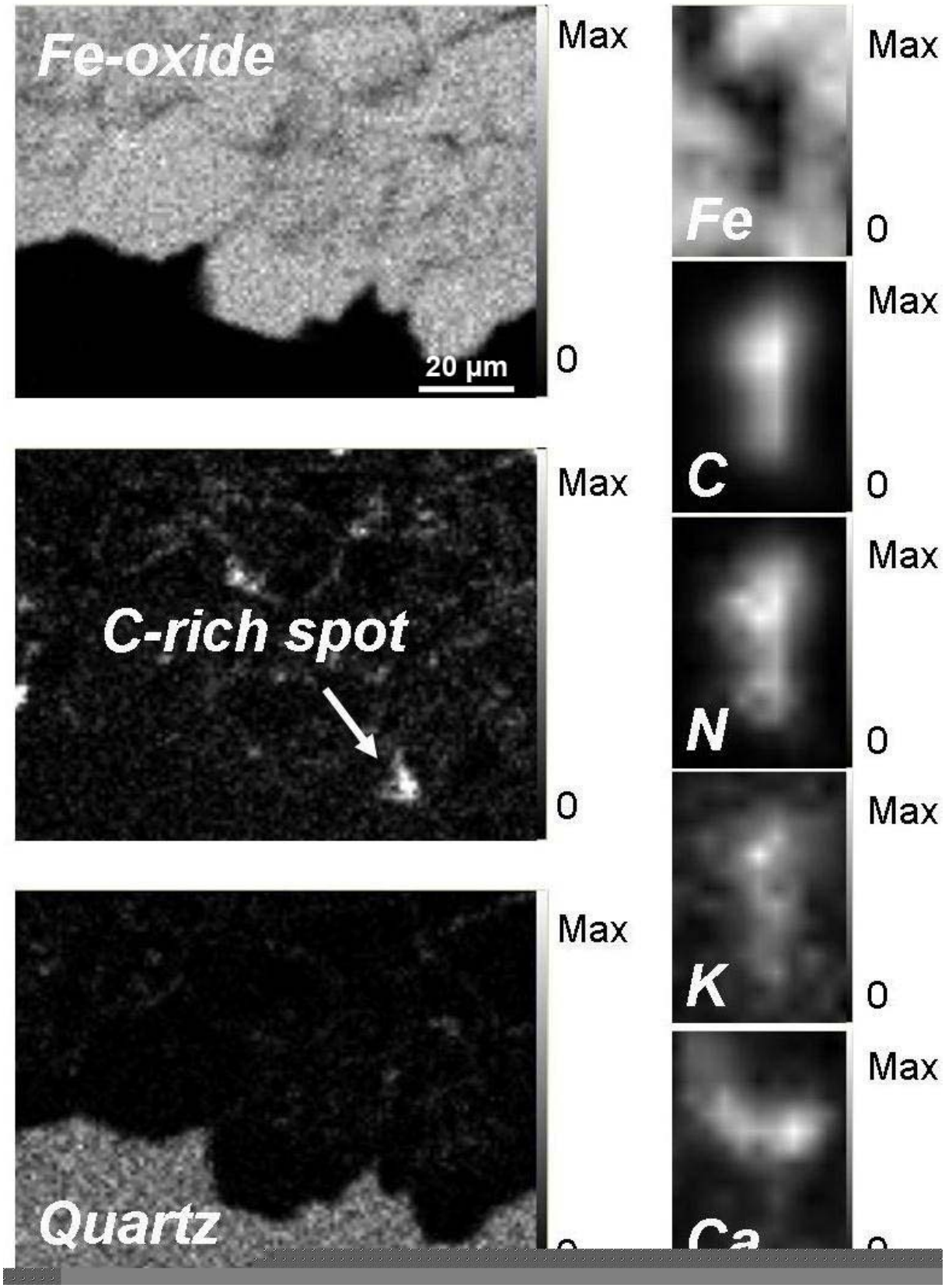
Fe-oxide
20 µm
Max
0
C-rich spot
Max
0
Quartz
Max
Fe
Max
0
C
Max
0
N
Max
0
K
Max
0
Ca
Max

Figure 6

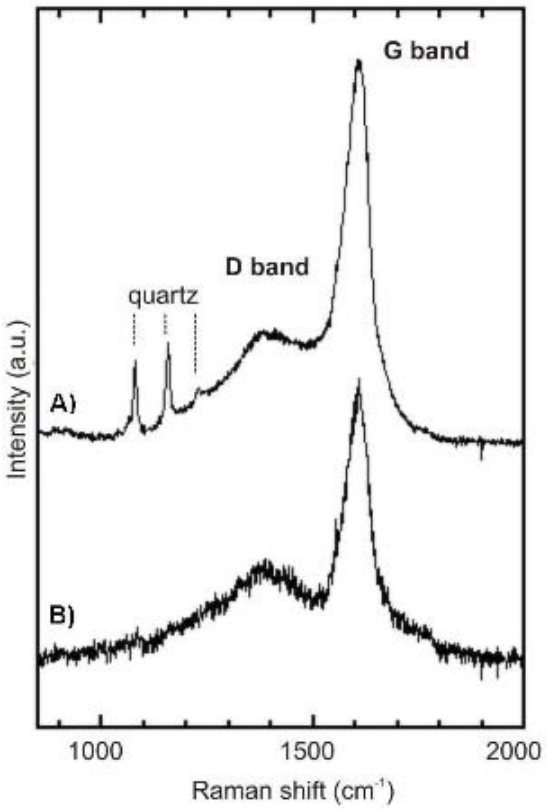
G band
D band
quartz
A)
B)
Intensity (a.u.)
1000
1500
2000
Raman shift (cm-1)

Figures 7

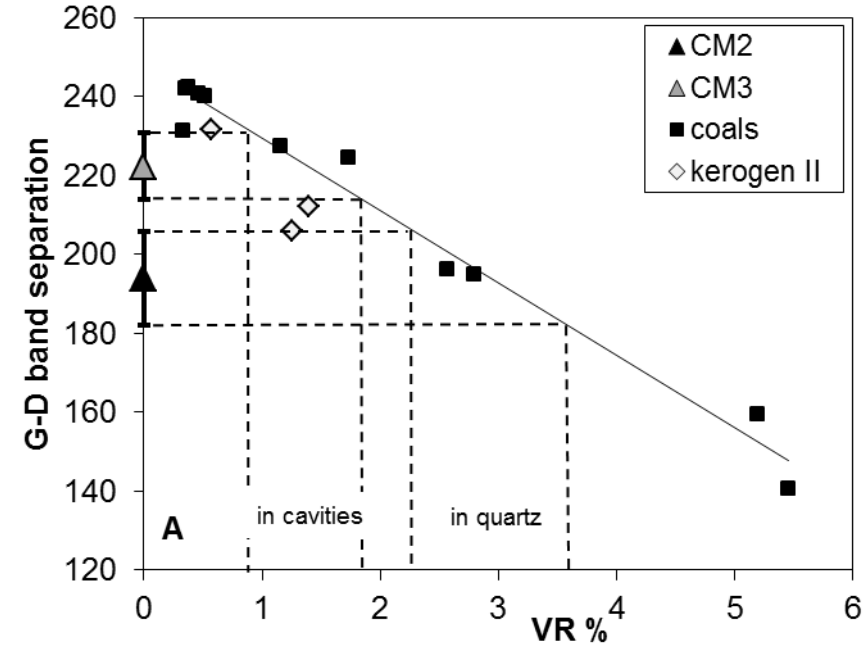
260
240
220
200
180
160
140
120
G-D band separation
A
in cavities
in quartz
CM2
CM3
coals
kerogen II
0
1
2
3
4
5
6
VR %

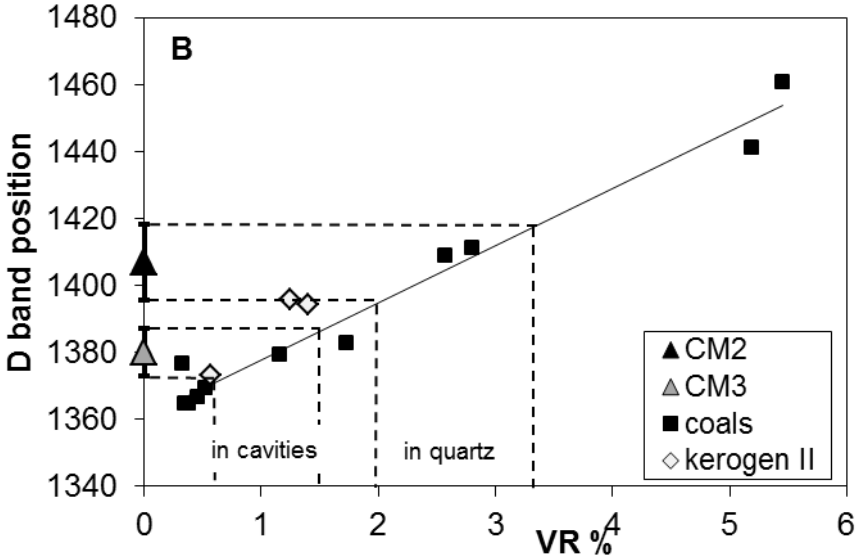
1480
1460
1440
1420
1400
1380
1360
1340
D band position
B
in cavities
in quartz
CM2
CM3
coals
kerogen II
0
1
2
3
4
5
6
VR %

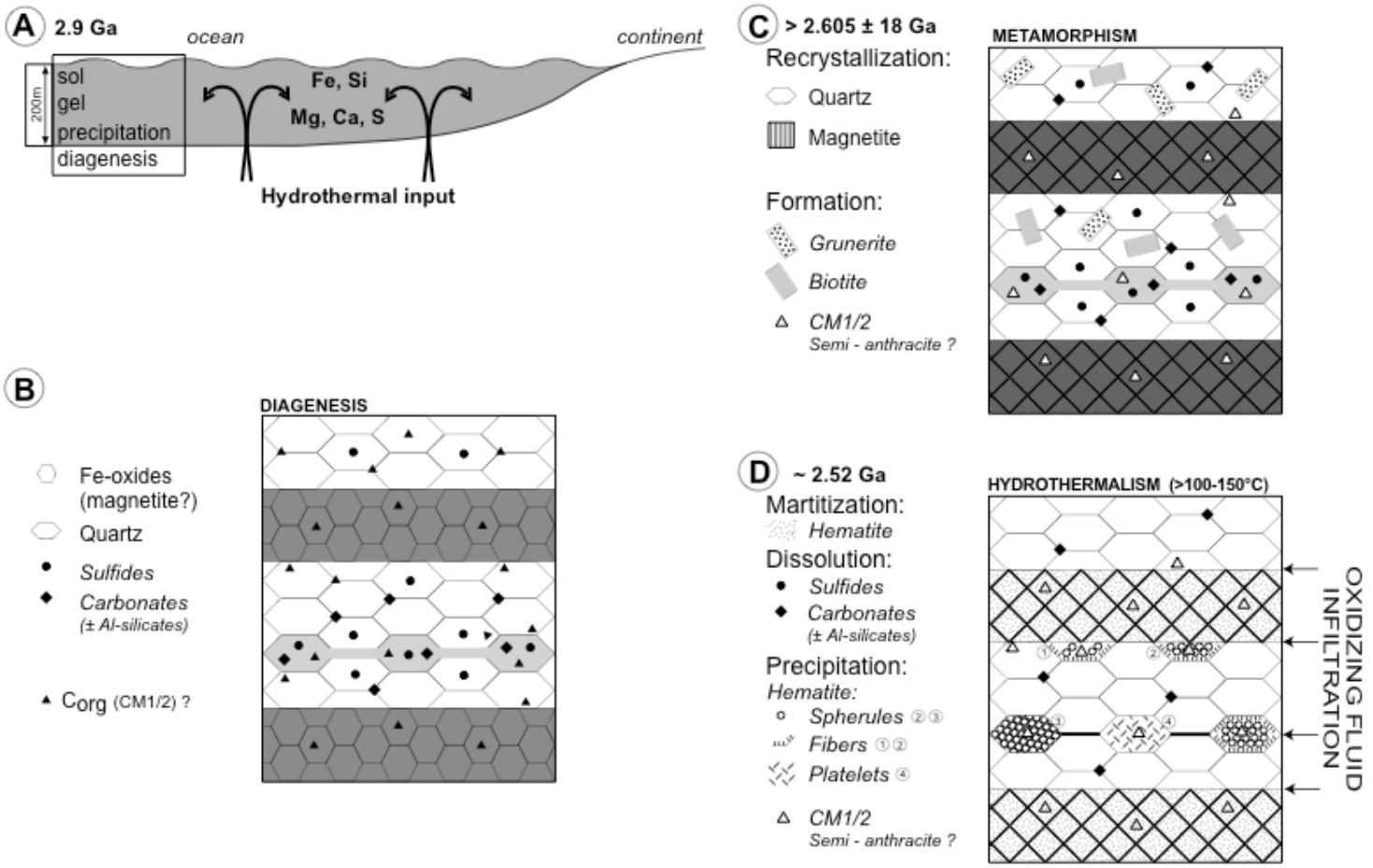
A
2.9 Ga
ocean
continent
200m
sol
gel
precipitation
diagenesis
Fe, Si
Mg, Ca, S
Hydrothermal input
B
DIAGENESIS
Fe-oxides
(magnetite?)
Quartz
Sulfides
Carbonates
(± Al-silicates)
Corg (CM1/2) ?
C
> 2.605 ± 18 Ga
Recrystallization:
Quartz
Magnetite
Formation:
Grunerite
Biotite
CM1/2
Semi - anthracite ?
METAMORPHISM
D
~ 2.52 Ga
Martitization:
Hematite
Dissolution:
Sulfides
Carbonates
(± Al-silicates)
Precipitation:
Hematite:
Spherules ②③
Fibers ①②
Platelets ④
CM1/2
Semi - anthracite ?
HYDROTHERMALISM (>100-150°C)
OXIDIZING FLUID
INFILTRATION

Figure 8

Table 1 + 2

TABLE 1. $\delta^{13}C$ values (± 0.2 %).

#	layer	$\delta^{13}C$
6	quartz	-23.87
9	Fe-oxide	-21.75
10	quartz	-24.24
11	Fe-oxide	-19.37
12	quartz	-24.66
15	quartz	-24.47
16	Fe-oxide	-19.98
17	quartz	-24.01
18	quartz	-23.32
19	quartz	-20.77
26	Fe-oxide	-20.19
	bulk	-24.03

: number of the different layers
of Figure 2A, except #26 not shown.

TABLE 2. Raman spectroscopy results for Indian carbonaceous matter (CM)

	pos G (cm^{-1})	std	FWHM-G	std	pos D (cm^{-1})	std	FWHM-D	std	G-D separ.	std	area ratio	std
CM2	1600.7	2.4	75.6	17.7	1406.8	11.3	243.6	35.5	193.9	12	1.2	0.3
CM3	1602.3	1.9	75.5	5	1379.9	7.3	256	53.8	222.3	8.5	1	0.2

Average values and standard deviation (std) of 16 pectra for CM disseminated in the quartz matrix (CM2)
and 25 spectra for CM found in the spherule-bearing cavities and around large hematitized magnetite (CM3).
Pos: peak position of the G and D bands; FWHM: Full Width Half Maximum; G-D separ: G-D band separation.